CHALMERS

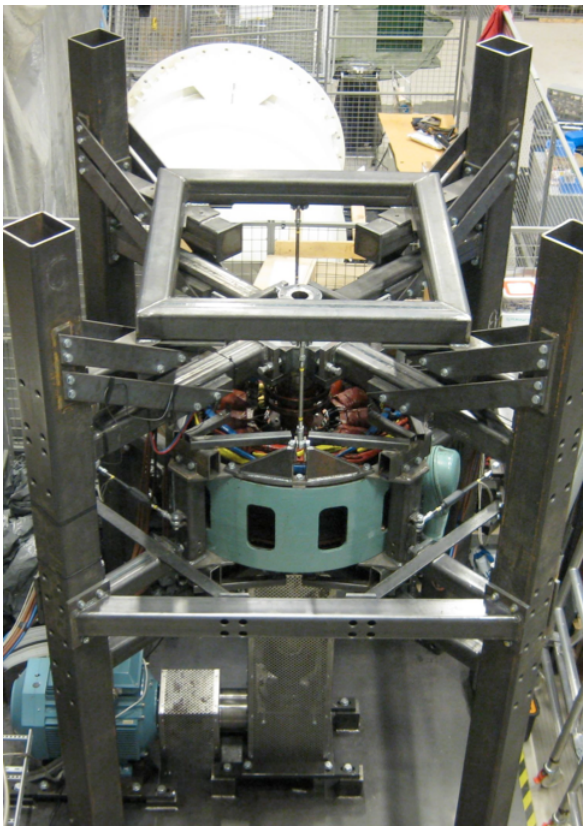

Electromagnetic Analysis of Rotating Permanent Magnet Exciters for Hydroelectric Generators

Master Thesis Project

JONAS NØLAND

Department of Energy and Environment
Division of Electric Power Engineering
CHALMERS UNIVERSITY OF TECHNOLOGY
Göteborg, Sweden 2013

Electromagnetic Analysis of Rotating Permanent Magnet Exciters for Hydroelectric Generators

Master Thesis Project

JONAS NØLAND

Department of Energy and Environment
Division of Electric Power Engineering
CHALMERS UNIVERSITY OF TECHNOLOGY
Göteborg, Sweden 2013

Electromagnetic Analysis of Rotating Permanent Magnet Exciters for
Hydroelectric Generators
Master Thesis Project
JONAS NøLAND

Department of Energy and Environment
Division of Electric Power Engineering
Chalmers University of Technology
SE–412 96 Göteborg
Sweden
Telephone +46 (0)31–772 1000

Cover:
Electromagnetic Analysis and Design of a Rotating Permanent Magnet Exciter for Hydroelectric Generator

Chalmers Bibliotek, Reproservice
Göteborg, Sweden 2013

Electromagnetic Analysis of Rotating Permanent Magnet Exciters for
Hydroelectric Generators
Master Thesis Project
JONAS NøLAND
Department of Energy and Environment
Division of Electric Power Engineering
Chalmers University of Technology

Abstract

The purpose of this project is to analyse different design possibilities for a rotating permanent magnet exciter for a hydroelectric generator. This is done through development of design models for optimizing suitable solutions. By use of Matlab/Simulink, COMSOL Multiphysics and ACE, the dynamics and the performance of the design is investigated. The aim is to have a robust system with low torque ripple absorbed by the exciter. It is shown that the six phase rectification solution has lower torque ripple for normal delay angles of the thyristor bridge compared to the three phase solution. For further development to try to reduce the torque ripple even more, one should optimize (reduce) the self and mutual inductances of the exciter rotor windings. A reduction of the parasitic magnetic energy storage in the system will reduce the torque ripple drastically.

Index Terms: Hydroelectric Generators, Permanent Magnet Machine Design, Finite Element Method, Thyristor Rectification Bridge

Acknowledgements

I would like to thank my supervisor Urban Lundin for his help and contribution throughout the project. He spent a lot of time to teach me how to use ACE and to program in FORTRAN. Urban gave a lot of good ideas during my project period. I would also like to thank my examiner Sonja Lundmark for following up the progression of the project and for giving me feedback on the report. The structure of the report would never been the same without numerous feedbacks from Sonja.

The Author
Göteborg, Sweden, 2013

Contents

List of Figures

Commonly used Acronyms

PM Permanent Magnet

EEC Electric Equivalent Circuit

MEC Magnetic Equivalent Circuit

FEA Finite Element Analysis

FDM Finite Difference Method

FEM Finite Element Method

Chapter 1

Introduction

1.1 Background

Hydropower still maintains its position as the most important source of renewable power generation in the world. In these days, most European countries go through a phase of intense refurbishment and upgrading of their existing plants. This leads to new challenges and the engineers need to gain back the knowledge that went lost twenty years ago. The trend in the hydropower industry today is more use of computerized tools and this has really revolutionized the whole design process.

The generator is one of the key components of a hydropower plant, since it is responsible for converting the mechanical energy from the fluid motion to magnetic energy through rotor excitation and finally to electric power absorbed by the stator windings, distributing the energy into the power grid. The generators used in hydro power plants are mainly synchronous generators. A whole generator system, the test rig Svante, is shown in figure 1.1, with a zoom of only the exciter part of the system (on the top) shown figure 1.2.

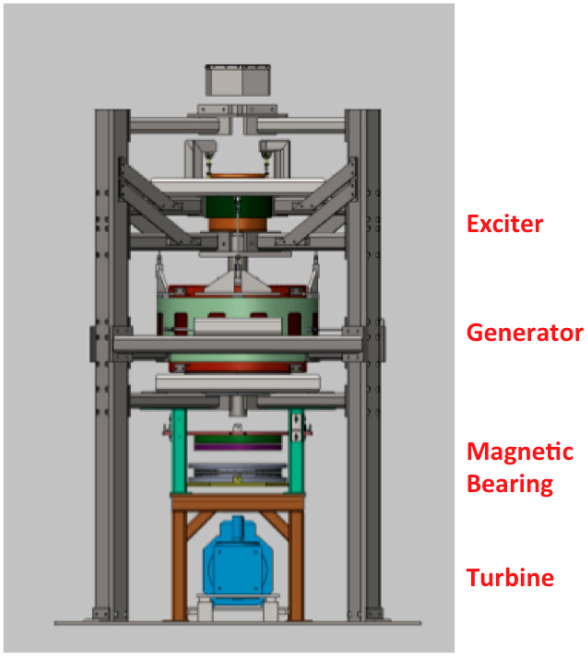

Fig. 1.1 Whole Hydroelectric Generation System

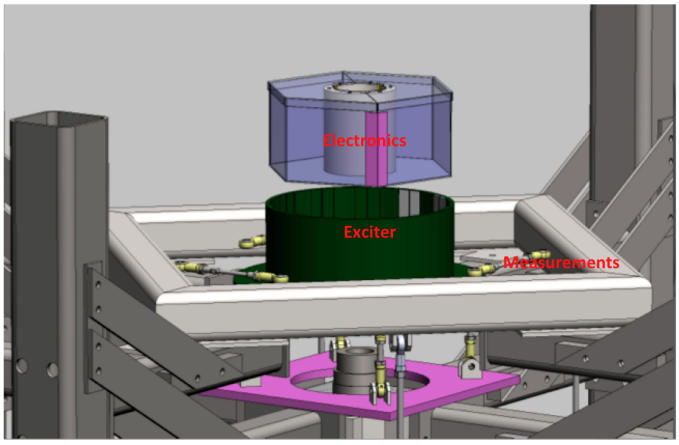

Fig. 1.2 Zoom on the Exciter

The excitation system of hydroelectric generators are either static or rotating. Both of them are available in the Svante test rig. The static system feeds dc current to the rotor of the generator through brushes. The rotating system, on the other hand, has permanent magnets in the stationary exciter stator that induces currents in the exciter rotor windings mounted on the rotating shaft. The currents are rectified before the connection to the rotor electromagnet of the generator. The static excitation principle is the most primitive one, but it is very easy to control. The fact that it acts very fast is a big advantage regarding the supply of reactive power reserves into the power grid, to maintain voltage stability. Because of the carbon dust from the brushes, you need regular maintenance of this part. That is an interesting economic aspect.

On the other side, the rotating excitation system is more complex, but it needs less equipment on the static side. The excitation current is transmitted brushlessly as a result of the induced currents on the rotor windings from the stationary permanent magnets on the stator side. The rectification is done by diodes on the rotor side and the rectified current is connected to the rotor winding of the main generator. The rotating solution is cheaper because of less cost for equipment and for maintenance. Because of high complexity, an in depth analysis is needed.

There is, however a possibility to join the advantages of a rotating exciter with the controllability of a static exciter by replacing the diodes mounted on the shaft with an active rectification system, in the easiest implementation made up of a 6-pulse thyristor rectification bridge (Figure 1.3). This means that one has to transfer a control signal to the shaft and thereby maneuver the thyristors.

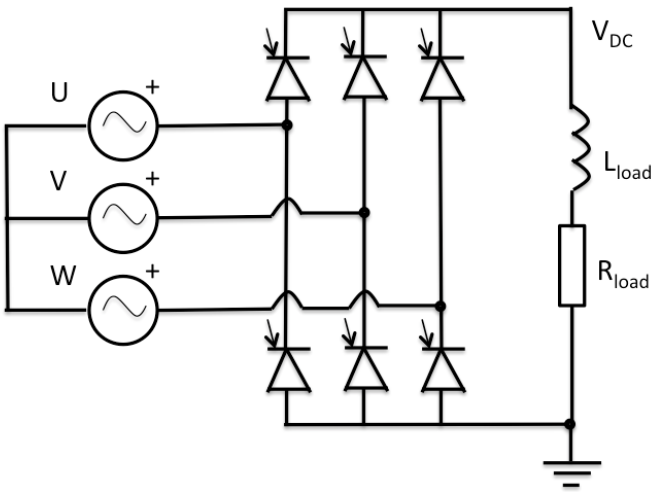

Fig. 1.3 Simplest form of active rectification system, 6 pulse thyristor bridge

The rotor winding of the main generator is then fed with a controllable DC current. The firing angles of the thyristor bridge are controlled wirelessly through Bluetooth communication. A pilot of the described excitation system has been installed at Bergeforsen Hydropower Station near Sundsvall, Sweden. The system has been shown to work well in operation, but vibrations is seen in the exciter with a bigger firing angle [5].

A complete diagram of the excitation system is shown in figure 1.4. The most important aspect is the flow of power between the different subsystems. It is important to note that it does not flow power from the permanent magnets in the stator. They only act as a catalyst for the energy conversion process. The power consumed is taken from the shaft connected to the hydroelectric turbine. The power generated in the rotor windings (6 individual phases) are fed into both the parasitic magnetic energy storage (inductive properties of the windings) and the dc load circuit through rectification. Because the current in the DC circuit is very stiff, the machine operation is close to the operation of a BLDC machine. The phase currents are not sinusoidal in shape and they will look more like square waves.

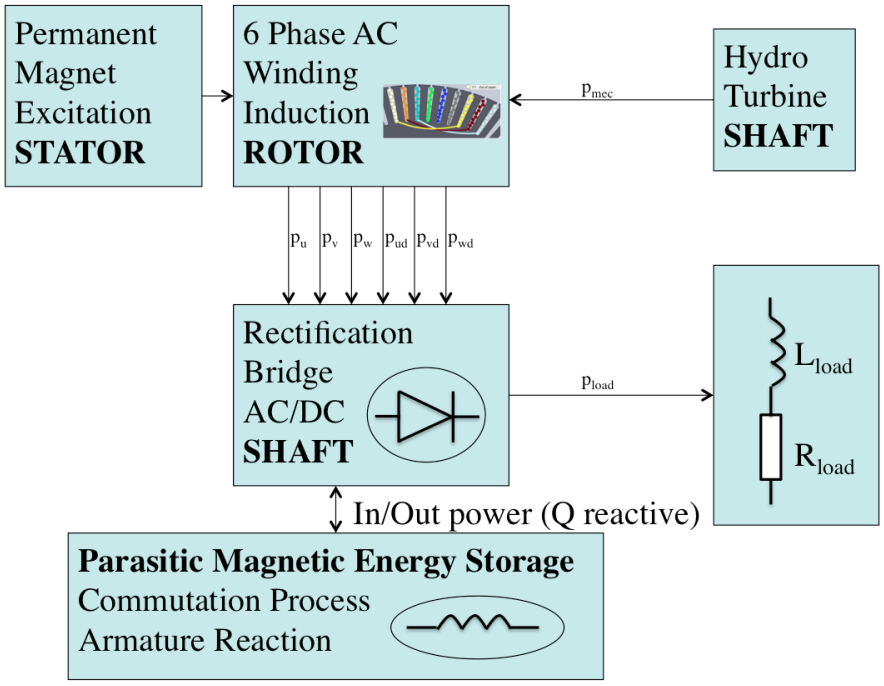

Fig. 1.4 Overall block diagram of the excitation system

The basic function of an excitation system is to provide direct current to the synchronous machine field winding on the rotor. In addition, the excitation system performs control and protective functions essential to the satisfactory performance of the power system by controlling the field voltage and thereby the field current. The control functions include the control of voltage and reactive power flow, and the enhancement of system stability. There is also protective functions to ensure that the capability limits of the synchronous machine, excitation system and the other equipment, are not exceeded. The basic requirement of the excitation system is to supply and automatically adjust the field current to maintain the terminal voltage of the synchronous generator. In addition, the excitation must be able to respond to transient disturbances with field forcing consistent with the generator instantaneous and short-term capabilities [13].

A magnetic field can be created in two different ways. Either a current through a winding generates the field or the field is sustained by a permanent magnet. Usually in a generator, the rotating magnetic field is generated by windings in order to be able to control the magnetic field excitation. For a smaller generator that creates the brushless rotating excitation, it is not so important to control the magnetic field. This is because you control for the current and not for the voltage. The current can be controlled by a rotating thyristor rectifier. Therefore permanent magnets can be used as excitation for the rotating exciter. If you still want some slow tuning of the magnetic field you can combine the permanent magnets with some windings. The field from a permanent magnet is not constant. It depends on the magnetic field path it follows. Another thing is that currents induced in

the windings that surrounds the permanent magnet, will create its own magnetic field, which will try to oppose the magnetic field from the permanent magnet. This is called the armature reaction.

1.2 Aim

The aim of the given master thesis project is to get a deep understanding of FEM methods applied to electromagnetic analysis of synchronous machines and how to couple them to external circuit equations. The work should be able to predict the electric, electromagnetic and mechanical behavior of the exciter and be in correspondence with experiments. The goal is to build up knowledge and to get a deeper understanding of the complexity behind the rotating exciter for hydropower applications.

1.3 Problem

There are several types of problems that need to be investigated in this thesis. The influence of the thyristor firing angle for the system should be analyzed. One major effect that needs to be studied is the current commutation process of the thyristor bridge. There are also stability issues regarding harmonics in the exciter AC system. The AC system has six phases, but can be reconnected into a 3-phase system. Different couplings between the phases during loaded operation need to be evaluated. An important comparison can be made if the exciter has 3 phases instead of 6. In the DC side of the exciter, both current and voltage levels will be investigated during operation. Also the power ripple generated in the rotor will be analyzed in order to predict the mechanical stability (especially the torque ripple). This ripple will depend on the interaction with the parasitic magnetic energy storage, originated in the magnetic properties of the rotor windings.

1.4 Scope

The thesis is focusing on the electromagnetic, power electronic and mechanical analysis. The mechanical analysis is only shortened down to the torque ripple investigation. Analysis of eigenfrequencies to avoid interactions with the environment is not done. The usage of FEM discretization in both time and space are important in the thesis. The control system of the exciter is out of the scope of this thesis, although it is closely related to the proposed analysis.

1.5 Method

A model for the thyristor controlled exciter was supposed to be developed in FORTRAN and integrated in the FEM software ACE, developed by ABB. Since it was hard to get the solution converged, ACE was instead used to find the time-dependent self and mutual inductances. This data from the FEM analysis was used to simulate the circuit in a self developed code in MATLAB/SIMULINK. Because the exciter core materials was far from saturated, the new approach gives good accuracy. The SIMULINK model forms a basis for control system evaluations. Comparisons is also made experimentally on the hydroelectric generator system available in the lab. This includes measurements of resistances and inductances.

Chapter 2

Machine Design Description

This chapter describes the machine design specifications of the excitation system investigated and it therefore forms the basis for the other chapters of this thesis.

A generator is an energy converter that converts rotational motion energy to electric energy. An exciter is also a generator because it generates the electrical energy needed to excite the rotor electromagnet of the main generator. In that sense, an exciter can be regarded as an energy converter as well. The energy you get out from the energy converter can never be higher than the amount of energy you put in. It is however a bit smaller and this is a because the energy conversion process consumes some energy. This byproduct of the conversion is known as losses. When you design a generator, you want to make the losses as small as possible. This is done through electromagnetic analysis.

Brushless permanent magnet generator design relies on the conversion of energy from mechanical to magnetic to electrical. Since the magnetic energy plays an important intermediate role in the energy conversion process, prediction of the magnetic field distribution is important to design a generator according to the specifications. There are a multiple of different methods to determine the magnetic field distribution within an apparatus. For very simple geometries, the distribution can be found analytically. However, the field distribution often has to be approximated. If the direction of the magnetic field is assumed to be known throughout the whole machine, the magnetic field can be calculated by magnetic circuit analysis, which is analogous to electric circuit analysis. A more accurate method to calculate both magnitude and direction is obtained by finite element analysis. Examples of possible methods are finite difference method, finite volume method and finite element method (See Appendix A7.1-A.4 for more information).

2.1 Maxwell's Equations

Maxwell's equations are of high importance when it comes to electrical machine design. The reference for the equations can be found in up to date design books [11].
Ampere's law:

$$\nabla \times \mathbf{H} = \mathbf{J} + \frac{\partial \mathbf{D}}{\partial t} \tag{2.1}$$

Faraday's law:

$$\nabla \times \mathbf{E} = -\frac{\partial \mathbf{B}}{\partial t} \tag{2.2}$$

Gauss's law:

$$\nabla \cdot \mathbf{D} = \rho \tag{2.3}$$

Continuity equation:

$$\nabla \cdot \mathbf{B} = 0 \tag{2.4}$$

Magnetization equation:

$$\mathbf{H} = \frac{\mathbf{B}}{\mu_0} - \mathbf{M} \tag{2.5}$$

Polarization equation:

$$\mathbf{D} = \epsilon_0 \mathbf{E} + \mathbf{P} \tag{2.6}$$

Linear, isotropic and non-dispersive materials:

$$\mathbf{B} = \mu_0 \mu_r \mathbf{H} \tag{2.7}$$

$$\mathbf{D} = \epsilon_0 \epsilon_r \mathbf{E} \tag{2.8}$$

where $\mathbf{B}$ is the magnetic flux density $[T]$, $\mathbf{H}$ is the magnetizing field $[A/m]$, $\mathbf{M}$ is the magnetization vector $[A/m]$, μ_0 is the permeability of free space $[H/m]$, μ_r is the relative permeability, $\mathbf{E}$ is the electric field $[N/C]$, $\mathbf{D}$ is the displacement field $[C/m^3]$, $\mathbf{P}$ is the polarization vector $[C/m^3]$, ϵ_0 is the permittivity of free space $[F/m]$, ϵ_r is the relative permittivity, $\mathbf{J}$ is the current density $[A/m^2]$.

2.2 Magnetic Circuits

The magnetic circuit approximation is always good to use in the first state of the electric machine design for rough estimates. For permanent magnet machine design, information about the hysteresis curve of the permanent magnet material is needed. The hysteresis curve for a permanent magnet is defined by equation 2.9 [6].

$$\mathbf{H} = \frac{\mathbf{B}}{\mu_0 \mu_r} - \mathbf{H_c} \tag{2.9}$$

The permeability of the permanent magnet can either be constant for all operating points or it can be a function of the local magnetic flux density. The equation is often written in terms of the reluctivity, just as in equation 2.10 [9].

$$\mathbf{H} = \nu(\mathbf{B})\mathbf{B} - \mathbf{H_c} \tag{2.10}$$

When the H-field is zero, the magnetic flux density is equal to the remanent flux. Then one obtains the following relation between the remanent flux and the coercive force [6]:

$$\mathbf{B_r} = \mu_0 \mu_r \mathbf{H_c} \tag{2.11}$$

The relation between the coercive force $\mathbf{H_c}$ and the remanence $\mathbf{B_r}$ gives the permeability of the permanent magnet. The remanent magnetic flux through the permanent magnet is the product of the remanence $\mathbf{B_r}$ and the cross sectional area $\mathbf{A_m}$ of the flux path in the permanent magnet. This is calculated for current source analogy (norton equivalent) in magnetic circuits [6].

$$\phi_\mathbf{r} = B_r A_m \tag{2.12}$$

The voltage source analogy (thevenin equivalent) in magnetic circuits is the magnetomotive force. It is the product of the coercive force and the permanent magnet length [6].

$$F_m = H_c l_m \tag{2.13}$$

The permanent magnet also has an internal resistance to the flow of the magnetic field, called reluctance (see equation 2.14). It depends on the linearized hysteresis curve of the permanent magnet [6].

$$\Re_m = \frac{l_m}{\mu_0 \mu_r A_m} \tag{2.14}$$

The magnetic conductance is the inverse of the reluctance, and it is called permeance [6].

$$P_m = \frac{\mu_0 \mu_r A_m}{r l_m} \tag{2.15}$$

The ohms law of magnetic circuits yields

$$\phi = \frac{F}{\Re} = PF \tag{2.16}$$

When solving the magnetic circuit, some of the flux is leaking, circulating in the shortest path around the permanent magnet. Since there is a lot of space for the flux to flow between the poles, it can be assumed that there is some leakage flux, which only circulates around the permanent magnets (See the leakage in figure 2.1). Total flux linkage through a coil depends on the number of turns, shown in equation 2.17 [6].

$$\Psi = N\phi \tag{2.17}$$

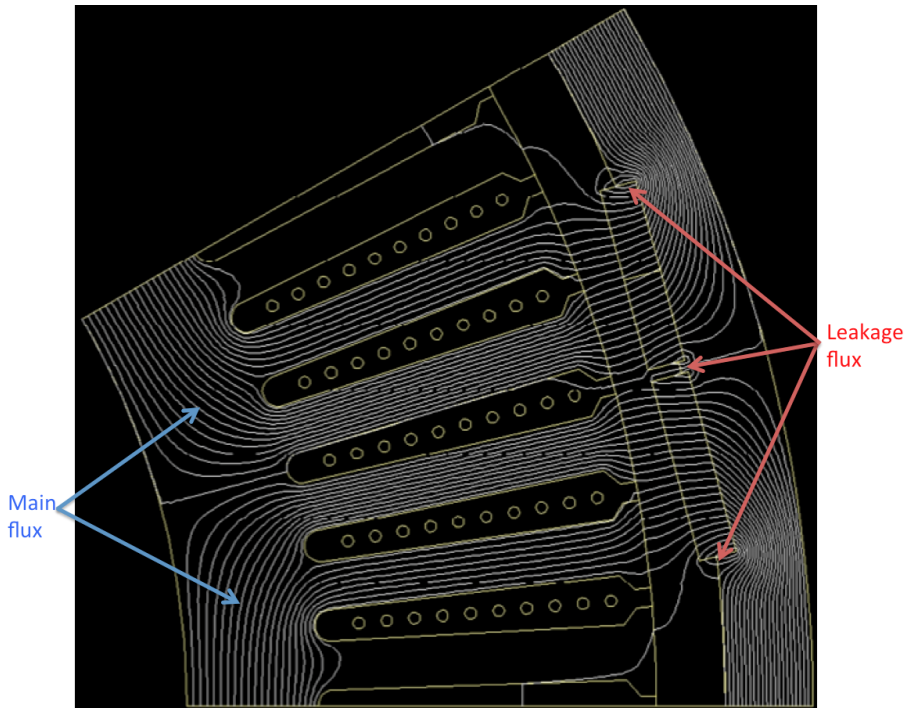

Fig. 2.1 Magnetic circuit of exciter (Explaination of the geometry in figure 2.3)

From the generalized form of Faraday's law, voltage induced in a coil is equal to the negative rate change of the flux linkage, which yields [6].

$$u = -\frac{d\Psi}{dt} \tag{2.18}$$

To calculate the no-load induced voltage, one let the permanent magnets rotate virtually with the solved static magnetic field. The rotation is discretized in time steps and the total flux linkage at every step is integrated. The voltage at every step can be approximated to be the flux linkage at the last step minus the flux linkage at the given step, divided by the time between. Another way is to find the induced voltage from the flux cutting version of faradays law for a conductor (equation 2.19 [6]).

$$u_{cond} = BLv \tag{2.19}$$

In equation 2.19, B is the magnetic flux density, L is the length of the conductor that cuts flux and v is the velocity of the conductor relative to the magnetic field. The equation relates the relative speed of the conductor to the magnetic field. Since the speed is rotational, the speed is equal to the product of the radius and the angular velocity. The angular velocity can be related to the nominal frequency and the number of poles. The induced electric field is:

$$E = Bv = B\omega R = \frac{2\pi R f B}{n_p} = -\frac{dA_z}{dt} \tag{2.20}$$

where E electric field induced along the conductor, ω is the angular velocity of the rotor conductor relative to the stator, R is the radius of the circle the conductor rotates, f is the electrical frequency, n_p is the number of pole pairs and A_z is the magnetic vector potential at the conductor cross section.

2.3 Design Specifications

From figure 2.2, one can define the geometry of the permanent magnets used in the exciter.

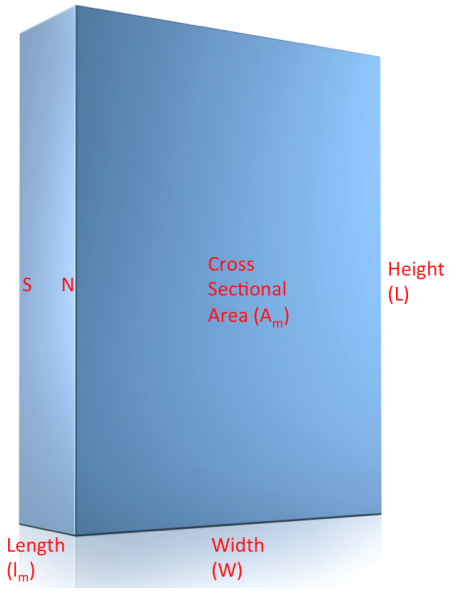

Fig. 2.2 Permanent Magnet Geometry

The given data for the permanent magnets are the following:

Remanence	Br	1.29T
Coercive force	Hc	977666 $\frac{A}{m}$
Relative permeability	μ_r	1.05
Length	l_m	6mm
Width	W	30mm
Height	L	200mm
Cross-Sectional Area	A_m	0.006 m^2
Internal Reluctance	$\Re_m$	757881 $\frac{A}{Wb}$
Internal Permeance	P_m	1.32 $\frac{\mu Wb}{A}$
Remanent flux	ϕ_r	7.74 mWb
Magnetomotive force	F_m	5866 A

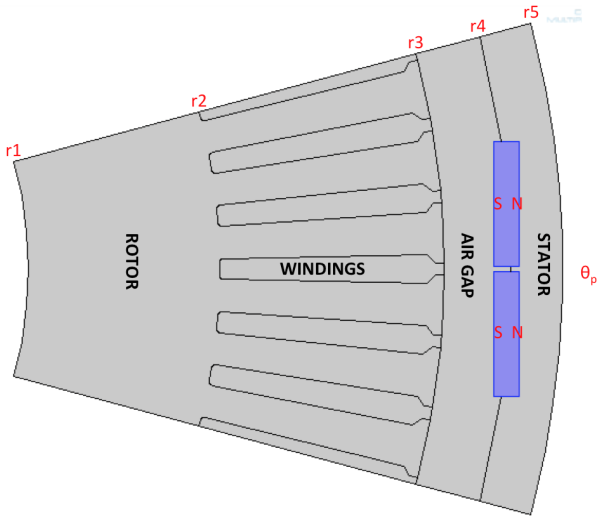

Fig. 2.3 One pole 2D geomtry

Figure 2.3 shows the 2D geometry of one pole of the exciter. The height of the 2D geometry is the same as the height of the permanent magnet shown in figure 2.2. The geometry has the following specifications:

Inner Rotor Radius	r1	0.1m
Inner Winding Radius	r2	0.145m
Outer Rotor Radius	r3	0.2m
Inner Stator Radius	r4	0.216m
Outer Stator Radius	r5	0.2285m
Minimum Air Gap Distance	g_{min}	12mm
Maximum Air Gap Distance	g_{max}	16mm
Pole Width	θ_p	$\frac{\pi}{6}$

For the given geometry, it is only needed to solve the magnetic circuit for half of the pole. This is because of symmetry and that the magnetic flux divide equally. Because the air gap distance is not uniform, the magnetic circuit calculation will vary to some degree compared to the numerical FEM solution. To solve the total magnetic circuit, the BH-curve in figure 2.4 should be used. Because of the non-linearity of the reluctivity in the material, the magnetic circuit should be solved by iterations. However, since the air gap is very large compared to other electrical machines, the reluctance of the iron cores will be negligible compared to the air gap reluctance. This makes the magnetic circuit calculations much simpler. The magnetic circuit consists of the internal reluctance of the source as well as the reluctance of the air gap. Since the air gap is not uniform in length, an averaged air gap distance should be found.

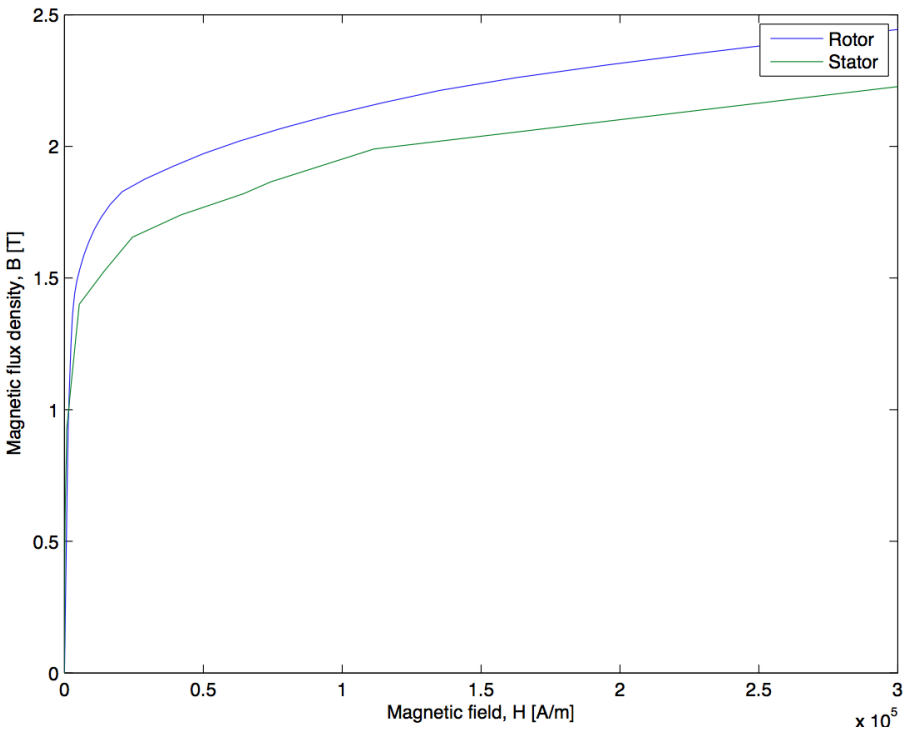

Fig. 2.4 BH curves

2.4 Resistance calculation

The resistance of a wire is governed by the following equation:

$$R = \frac{l}{\sigma A} \tag{2.21}$$

Since the machine is split into two parallel circuits, the total area becomes two times the conductor area. Equation 2.21 modifies to

$$R = \frac{l}{2\sigma A_c} \tag{2.22}$$

where

$$A_c = \frac{1}{4}\pi D_c^2 \tag{2.23}$$

The total length of the wire through half of the machine is proportional to the length per turn (l_t), the number of conductors per coil (N) and the number of series connected coils, which yields

$$l = 6Nl_t \tag{2.24}$$

where

$$l_t = 2l_z + 2l_e \tag{2.25}$$

and

$$l_e = \theta_p \frac{r_2 + r_3}{2} + \frac{l_h - l_z}{4} \tag{2.26}$$

The generalized formula becomes

$$R = \frac{6N(3l_z + l_h + \theta_p \frac{r_2+r_3}{2})}{\sigma\pi D_c^2} \tag{2.27}$$

where the parameters and calculations are described below

Conductor Diameter	D_c	3mm
Conductor Area	A_c	$7.07 \cdot 10^{-6} m^2$
Conductivity Copper	σ	$5.96 \cdot 10^7 \frac{S}{m}$
Number of turns per coil	N	12
Length of the copper tubes in the rotor	l_z	0.2m
Total height of the rotor	l_h	0.35m
Average conductor end turn length	l_e	$0.13m$
Average length per conductor turn	l_t	$0.66m$
Total conductor length through half machine	l	$47.2m$
Resistance per phase	R	$56m\Omega$

The measured resistance per phase was $62.5m\Omega$ (from the rotor shown in figure 2.5), which gives an accuracy of 10 percent compared to the calculated value.

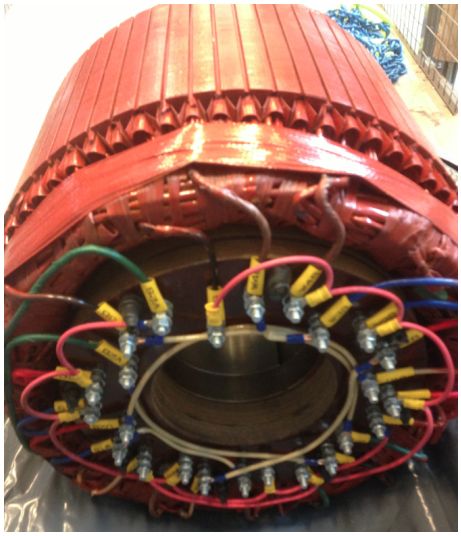

Fig. 2.5 Prototype of the Rotor

2.5 Inductance calculation

A simplified analytical model for the inductance calculation is used where the iron core reluctance is neglected [7]. The slot model is shown in figure 2.6. The magnetic field through the slot is calculated for every y-coordinate based on the slot distance and the fact that the $Ampère$ loop experiences no MMF drop over the iron core.

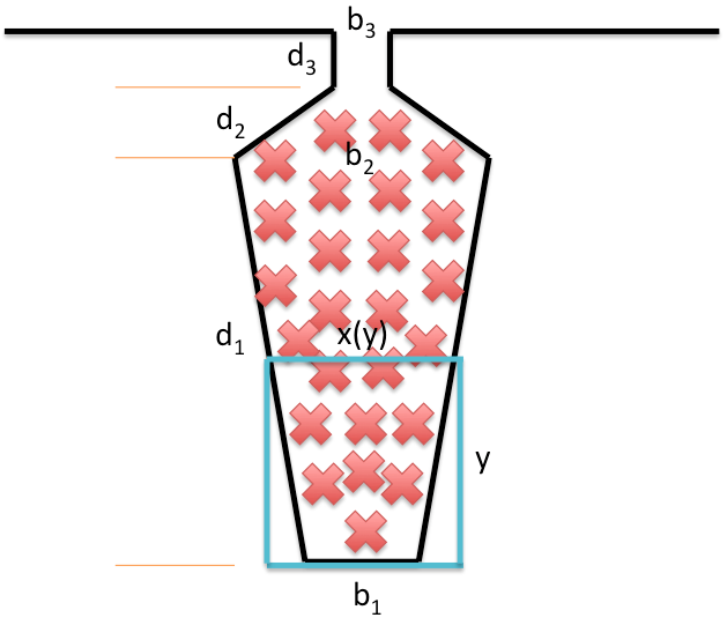

Fig. 2.6 Slot inductance model

The integral form of $Ampère's$ law states that

$$\oint \vec{H}\vec{dl} = I_{enc} \tag{2.28}$$

which simplifies to

$$H_x(y)x(y) = I_{enc}(y) \tag{2.29}$$

and further to

$$B_x(y) = \frac{\mu_0 I_{enc}(y)}{x(y)} \tag{2.30}$$

The slot width for a given y-coordinate is linearized to

$$x(y) = b_1 + \frac{b_2 - b_1}{d_1} y \tag{2.31}$$

for $0 =< y < d_1$, to

$$x(y) = b_2 + \frac{b_3 - b_2}{d_2}(y - d_1) \tag{2.32}$$

for $d_1 =< y < (d_1 + d_2)$, and to

$$x(y) = b_3 \tag{2.33}$$

for $(d_1 + d_2) =< y =< (d_1 + d_2 + d_3)$. The net current enclosed for a given y-coordinate can be approximated by the total current in the slot multiplied with the ratio of the conductor area enclosed by the $Ampère$ loop to the total conductor area of the slot. This yields

$$Ienc(y) = \frac{A(y)}{A_{tot}} N_s I \tag{2.34}$$

Insertion of equation 2.34 into equation 2.30 yields

$$B_x(y) = \frac{\mu_0 N_s I}{A_{tot}} \frac{A(y)}{x(y)} \tag{2.35}$$

where

$$A_{tot} = \frac{b_1 + b_2}{2} d_1 + \frac{b_2 + b_3}{2} d_2 \tag{2.36}$$

and

$$A(y) = \int_0^y x(y) dy \tag{2.37}$$

The solved integral gives

$$A(y) = b_1 y + \frac{b_2 - b_1}{2d_1} y^2 \tag{2.38}$$

for $0 =< y < d_1$, and

$$A(y) = \left[b_2 - \frac{d_1}{d_2}(b_3 - b_2) \right] y + \frac{b_3 - b_2}{2d_2} y^2 + \frac{b_1 + b_2}{2} d_1 \tag{2.39}$$

for $d_1 =< y < (d_1 + d_2)$, and

$$A(y) = A_{tot} \tag{2.40}$$

for $(d_1 + d_2) =< y =< (d_1 + d_2 + d_3)$. A infinitesimal flux contribution can be calculated from the product of magnetic flux density in a point and the infinitesimal area, which yields

$$d\phi = B_x(y) l_z dy \tag{2.41}$$

To get the flux linkage, one needs to take into the account the number of turns the flux encloses, which yields

$$d\lambda = n(y) B_x(y) l_z dy \tag{2.42}$$

The number of turns a y-coordinate encloses can be approximated in the same way as for the calculation of the enclosed current. This gives

$$n(y) = \frac{A(y)}{A_{tot}} N_s \tag{2.43}$$

Insertion of equation 2.35 and equation 2.43 into equation 2.42 yields

$$d\lambda = \frac{\mu_0 N_s^2 I l_z}{A_{tot}^2} \frac{A(y)^2}{x(y)} dy \tag{2.44}$$

The total flux linkage can be calculated as the product of the inductance of a slot and the current flowing, which yields

$$\lambda = LI \tag{2.45}$$

and in the differential form

$$dL = \frac{d\lambda}{I} \tag{2.46}$$

which eliminates the current when you substitute the differential flux linkage into the differential inductance equation. This gives

$$\frac{dL}{dy}(y) = \frac{\mu_0 N_s^2 l_z}{A_{tot}^2} \frac{A(y)^2}{x(y)} \tag{2.47}$$

The differential inductance equation should be integrated over the three defined slot regions. The total slot inductance will then be the sum of the inductance from the three regions multiplied with a factor three. The factor three comes from the fact that six slots are series connected and the fact that this inductance is parallel connected with an identical inductance. This gives

$$L_{slot} = 3(L_1 + L_2 + L_3) \tag{2.48}$$

The integrals to be solved are:

$$L_1 = \int_0^{d_1} \left[\frac{dL}{dy}(y) \right] dy \tag{2.49}$$

and

$$L_2 = \int_{d_1}^{d_1 + d_2} \left[\frac{dL}{dy}(y) \right] dy \tag{2.50}$$

and

$$L_3 = \int_{d_1+d_2}^{d_1+d_2+d_3} \left[\frac{dL}{dy}(y)\right] dy \tag{2.51}$$

The first integral is solved by the substitution of the inductance derivative for region 1, which yields

$$L_1 = \frac{\mu_0 N_s^2 l_z}{A_{tot}^2} \int_0^{d_1} \frac{(b_1 y + \frac{b_2-b_1}{2d_1} y^2)^2}{b_1 + \frac{b_2-b_1}{d_1} y} dy \tag{2.52}$$

The integral simplifies by polynomial division

$$L_1 = \frac{\mu_0 N_s^2 l_z}{A_{tot}^2} \left[\int_0^{d_1} (b_1 y^2 + \frac{b_2 - b_1}{4d_1} y^3) dy - \frac{b_1(b_2-b_1)}{4} \int_0^{d_1} \frac{y^3}{d_1 b_1 + (b_2 - b_1)y} dy \right] \tag{2.53}$$

to finally

$$L_1 = \frac{\mu_0 N_s^2 l_z d_1^3}{A_{tot}^2} \left[\frac{9b_1}{48} + \frac{b_2}{16} + \frac{b_1^2}{8(b_2-b_1)} - \frac{b_1^3}{4(b_2-b_1)^2} + \frac{b_1^4}{4(b_2-b_1)^3} ln(\frac{b_2}{b_1}) \right] \tag{2.54}$$

In a similar way integral 2 is solved

$$L_2 = \frac{\mu_0 N_s^2 l_z}{A_{tot}^2} \int_{d_1}^{d_1+d_2} \frac{(\left[b_2 - \frac{d_1}{d_2}(b_3 - b_2)\right] y + \frac{b_3-b_2}{2d_2} y^2 + \frac{b_1+b_2}{2} d_1)^2}{b_2 - \frac{d_1}{d_2}(b_3 - b_2) + \frac{b_3-b_2}{d_2} y} dy \tag{2.55}$$

and by switching the integral boundaries, the integral simplifies to

$$L_2 = \frac{\mu_0 N_s^2 l_z}{A_{tot}^2} \int_0^{d_2} \frac{(b_2 y + \frac{b_3-b_2}{2d_2} y^2 + \frac{b_1+b_2}{2} d_1)^2}{b_2 + \frac{b_3-b_2}{d_2} y} dy \tag{2.56}$$

Finally one will end up with

$$L_2 = \frac{\mu_0 N_s^2 l_z d_2}{4A_{tot}^2} (C1 + C2 + C3) \tag{2.57}$$

where

$$C1 = d_2^2 \left(\frac{b_2(2b_2 d_1 - b_2 d_2 - 2b_3 d_1)}{2d_2(b_2 - b_3)} + b_1 \frac{d_1}{d_2} + b_2 - \frac{b_2 - b_3}{4} \right) \tag{2.58}$$

and

$$C2 = -b_2 d_2 \frac{2b_1 d_1 (b_2 - b_3) + b_2(b_2(2d_1 + d_2) - 2b_3 d_1)}{(b_2 - b_3)^2} \tag{2.59}$$

and

$$C3 = \frac{(b_1 d_1 (b_2 - b_3) + b_2(b_2(d_1 + d_2) - b_3 d_1))^2}{(b_2 - b_3)^3} ln(\frac{b_2}{b_3}) \tag{2.60}$$

The last region is very simple to calculate, and yields

$$L_3 = \mu_0 N_s^2 l_z \frac{d_3}{b_3} \tag{2.61}$$

One will also have leakage inductance in the air gap as in the slot. However, here the air gap $Ampère$ loop is approximated by the slot opening plus two half circles as shown in figure 2.7.

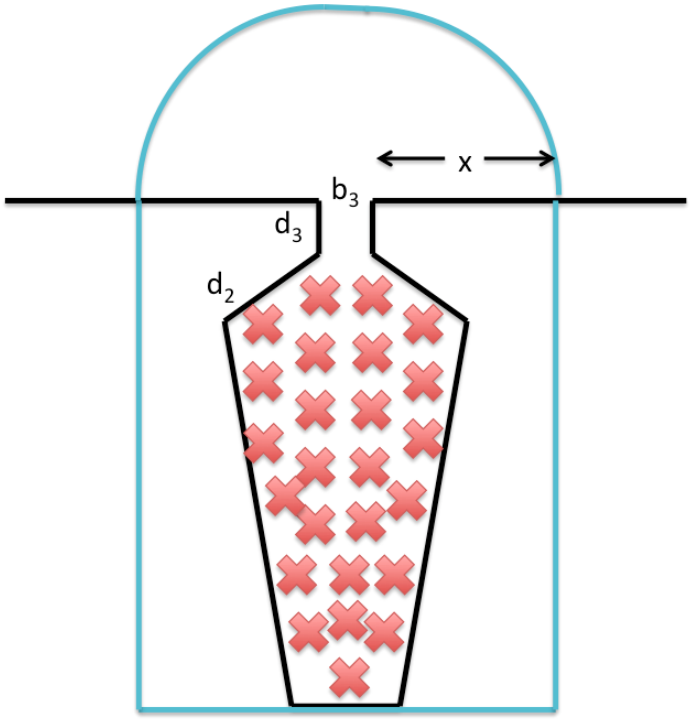

Fig. 2.7 Leakage inductance model

The $Ampère$ loop can be used in a differential permeance model, given by the length for each permeance element. This gives

$$l(x) = \pi x + b_3 \tag{2.62}$$

where

$$dP = \frac{\mu_0 l_z dx}{l(x)} \tag{2.63}$$

and

$$dL = N_s^2 \frac{\mu_0 l_z}{\pi x + b_3} dx \tag{2.64}$$

The leakage inductance without the stator should be integrated over the whole pole pitch, which yields

$$L_{\sigma *} = \mu_0 N_s^2 l_z \int_0^{\frac{w_p}{2}} \frac{1}{\pi x + b_3} dx \tag{2.65}$$

and finally

$$L_{\sigma *} = \frac{\mu_0 N_s^2 l_z}{\pi} ln(1 + \frac{\pi w_p}{2b_3}) \tag{2.66}$$

which gives the total inductance of

$$L_{ph*} = 3(L_s + L_{\sigma *}) \tag{2.67}$$

The leakage inductance becomes smaller when the stator is in place. Then more permeance lines will be directed through the stator. Therefore the leakage with stator is only integrated over the air gap length, which yields

$$L_\sigma = \frac{\mu_0 N_s^2 l_z}{\pi} ln(1 + \frac{\pi g}{b_3}) \tag{2.68}$$

The inductance with stator can be calculated by magnetic circuit analysis given by figure 2.8.

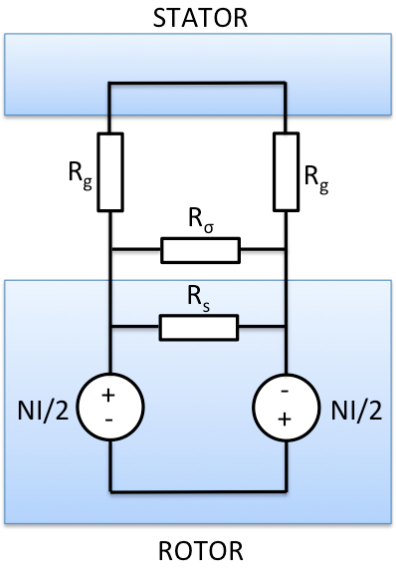

Fig. 2.8 Magnetic circuit for the inductance calculation with stator in place

The two air gap reluctances can be calculated as

$$\Re_g = \frac{ln(1+\frac{g}{r3})}{\mu_0 l_z \frac{\theta_p}{2}} \tag{2.69}$$

The solution to the magnetic circuit with respect to the inductance is

$$L_{ph} = 3N^2 \left(\frac{1}{\Re_s} + \frac{1}{\Re_\sigma} + \frac{1}{2\Re_g} \right) \tag{2.70}$$

Values of the parameters and the calculations are given below

Rotor pole width	w_p	104.7mm
Bottom rotor slot width	b_1	5mm
Upper rotor slot width	b_2	8mm
Rotor teeth opening	b_3	3mm
Rotor slot radial length	d_1	50mm
Bottom rotor teeth height	d_2	2mm
Top rotor teeth height	d_3	2mm
Number of conductors per slot	N_s	24
Total slot conductor area	A_{tot}	$3.36 \cdot 10^{-4} m^2$
Permeability of free space	μ_0	$4\pi 10^{-7} \frac{H}{m}$
Slot leakage inductance 1	L_1	$276.79 \mu H$
Slot leakage inductance 2	L_2	$55.52 \mu H$
Teeth slot leakage inductance	L_3	$96.51 \mu H$
Total slot leakage inductance	L_s	$428.82 \mu H$
Air gap leakage inductance (Without stator)	$L_{\sigma *}$	$185.34 \mu H$
Air gap leakage inductance (With stator)	L_σ	$103.14 \mu H$
Total per phase rotor inductance (without stator)	L_{ph*}	$1.8 mH$
Slot reluctance	$\Re_s$	$1.3432 \cdot 10^6 \frac{A-turns}{Wb}$
Air gap leakage reluctance (without stator)	$\Re_{\sigma *}$	$3.1078 \cdot 10^6 \frac{A-turns}{Wb}$
Air gap leakage reluctance (with stator)	$\Re_\sigma$	$5.5845 \cdot 10^6 \frac{A-turns}{Wb}$
Air gap reluctance (with stator)	$\Re_g$	$1.1697 \cdot 10^6 \frac{A-turns}{Wb}$
Total per phase rotor inductance (with stator)	L_{ph}	$2.3 mH$

Since the stator has not been built yet, the self inductance was measured without the stator. The inductance

was measured at 100Hz to be 1.5mH. This is within an accuracy of 20 percent compared to the analytically calculated value (1.8mH). From the inductance calculation model it is possible to vary some design parameters to see how sensitive the self inductance are to those. Figure 2.9, 2.10 and 2.11 shows how the inductance changes with air gap, turns and slot opening (Carter's factor are neglected for the slot opening since the slot pitch is relatively large).

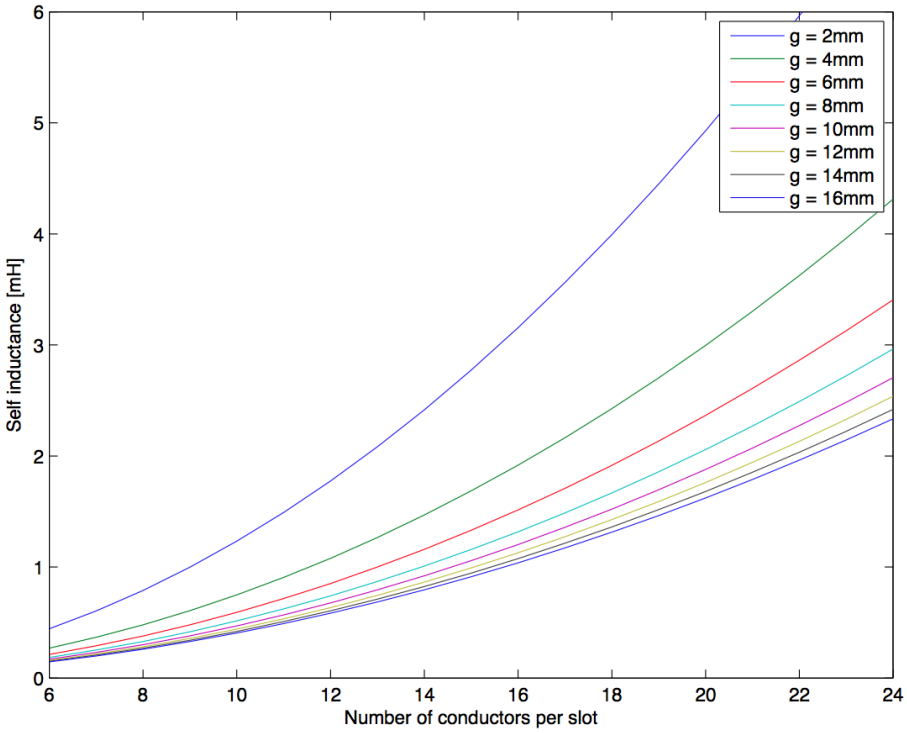

Fig. 2.9 Self inductance sensitivity to number of conductors per slot and the air gap distance

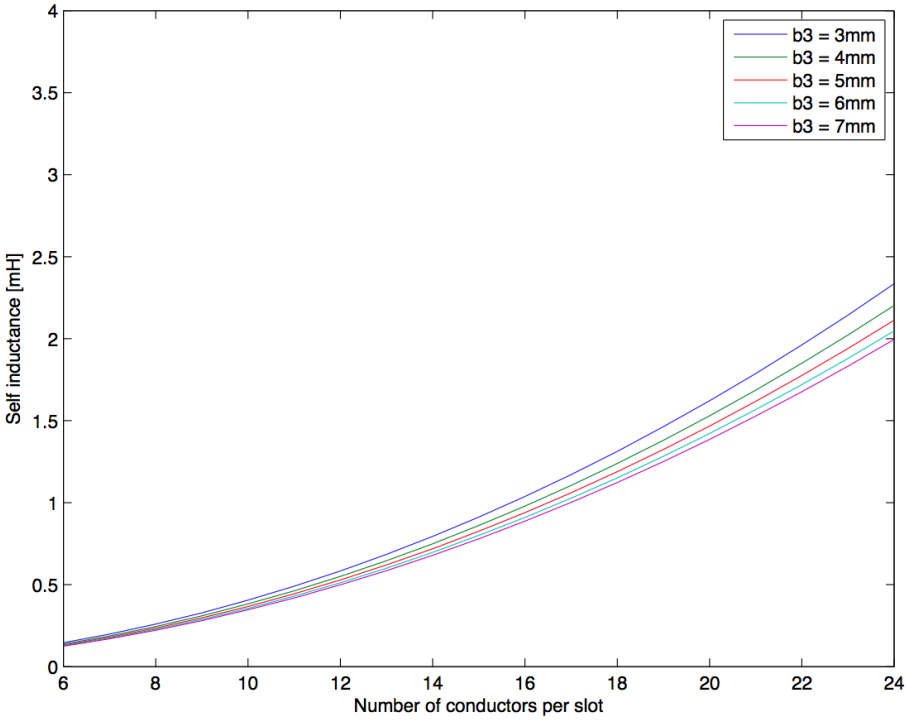

Fig. 2.10 Self inductance sensitivity to number of conductors per slot and the slot opening with 16 mm air gap

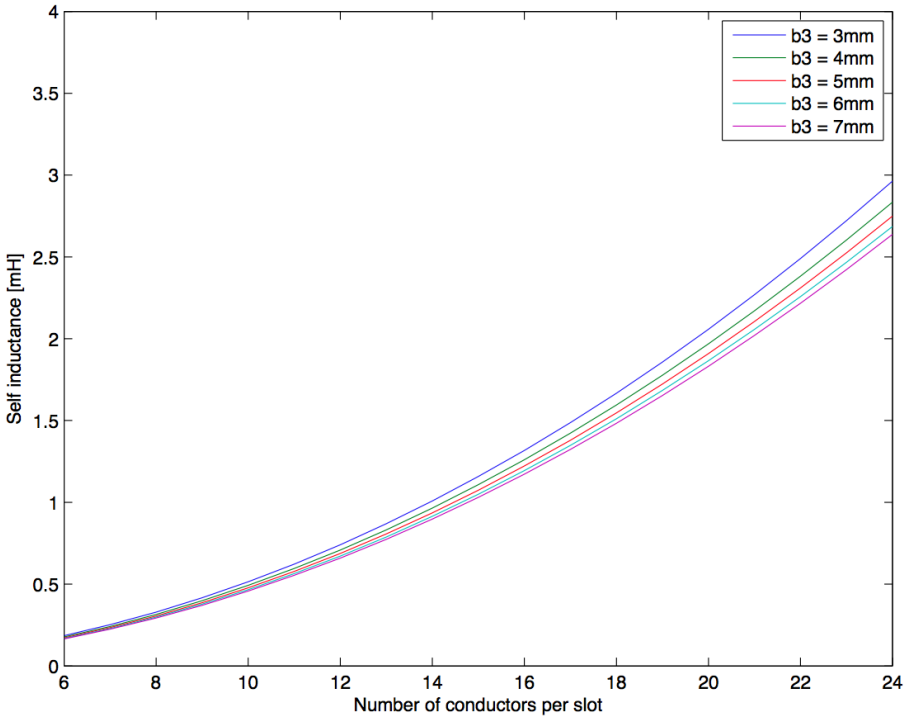

Fig. 2.11 Self inductance sensitivity to number of conductors per slot and the slot opening with 8 mm air gap

It can be shown that less number of turns reduce the self inductance drastically. A bigger slot opening will reduce the inductance significantly less. Another issue with a bigger slot opening is that the cogging torque will increase. The cogging torque are given by the following formula [11]:

$$T_{cogging} = \frac{dW_{mag,PM}}{d\theta_{mec}} \tag{2.71}$$

where $W_{mag,PM}$ is the magnetic energy generated from the permanent magnets in the stator and θ_{mec} is the mechanical angular position. The cogging torque can be found through FEM by calculating the magnetic energy for multiple angular positions. With low stepping the derivative of the magnetic energy with respect to the angular position can be approximated.

Chapter 3

Finite Element Analysis

The finite element analysis for a generator is often obtained in 2D, to simplify the analysis. Either scalar magnetic potential or magnetic vector potential is solved directly to obtain the magnetic flux distribution. This is much simpler than to try to find the magnetic field distribution directly. If the B-field should be directly solved in 2D, two vector components should be obtained in every point.

3.1 Magnetic scalar potential

Magnetic ohm's law [12]:

$$\mathbf{B} = \mu\mathbf{H} = -\mu_0\mu_r\nabla\Omega \tag{3.1}$$

Electric ohm's law [12]:

$$\mathbf{J} = \sigma\mathbf{E} = -\sigma\nabla V \tag{3.2}$$

The magnetic scalar potential (Ω) is analogous to electric voltage potential, and describes the magnetomotive force (ampere-turns) in a certain point. In the same way voltage is the driving force for current; magnetic scalar potential is the driving force for magnetic flux. Often in generators, the windings are designed to create a sinusoidal MMF-distribution in order to produce a sinusoidal voltage when current flows in the windings (armature reaction).

$$\frac{\partial B_x}{\partial x} + \frac{\partial B_y}{\partial y} + \frac{\partial B_z}{\partial z} = 0 \tag{3.3}$$

From equation 3.3 [12] (magnetic continuity equation), the diffusion equation for scalar potential can be derived:

$$\frac{\partial}{\partial x}\left[\mu_0\mu_r\frac{\partial\Omega}{\partial x}\right] + \frac{\partial}{\partial y}\left[\mu_0\mu_r\frac{\partial\Omega}{\partial y}\right] + \frac{\partial}{\partial z}\left[\mu_0\mu_r\frac{\partial\Omega}{\partial z}\right] = 0 \tag{3.4}$$

Laplace equation is obtained if the relative permeability is constant:

$$\frac{\partial^2\Omega}{\partial x^2} + \frac{\partial^2\Omega}{\partial y^2} + \frac{\partial^2\Omega}{\partial z^2} = 0 \tag{3.5}$$

In the 2D analysis, the z-dependent part of the equation is neglected.

3.2 Magnetic Equivalent Circuit Method

The equation for the scalar magnetic potential can be discretized by integrating up rectangular "volumes" [1]. In 2D analysis, the "volume" is integrated in both x and y direction, as in equation 3.6.

$$\int_s^n\int_w^e \frac{\partial}{\partial x}\left[\mu\frac{\partial\Omega}{\partial x}\right]dxdy + \int_s^n\int_w^e \frac{\partial}{\partial y}\left[\mu\frac{\partial\Omega}{\partial y}\right]dxdy = 0 \tag{3.6}$$

$$\left(\left[\mu\frac{\partial\Omega}{\partial x}\right]_e - \left[\mu\frac{\partial\Omega}{\partial x}\right]_w\right)\Delta y + \left(\left[\mu\frac{\partial\Omega}{\partial y}\right]_n - \left[\mu\frac{\partial\Omega}{\partial y}\right]_s\right)\Delta x = 0 \tag{3.7}$$

$$\left[\frac{\mu_e\Delta y}{\partial x_e}\right](\Omega_E - \Omega_P) - \left[\frac{\mu_w\Delta y}{\partial x_w}\right](\Omega_P - \Omega_W) + \left[\frac{\mu_n\Delta x}{\partial y_n}\right](\Omega_N - \Omega_P) - \left[\frac{\mu_s\Delta x}{\partial y_s}\right](\Omega_P - \Omega_S) = 0 \tag{3.8}$$

It turns out that the constants multiplied with the potential differences is equal to the permeance per meter, the inverse of the reluctance. Equation 3.9 then describes a network of mutual permeances.

$$P_e(\Omega_P - \Omega_E) + P_w(\Omega_P - \Omega_W) + P_n(\Omega_P - \Omega_N) + P_s(\Omega_P - \Omega_S) = 0 \tag{3.9}$$

Finally the equation looks like a reluctance network of "flux tubes" where Kirchhoffs current law for magnetic flux is fulfilled (equation 3.10). It describes how the magnetic equivalent circuit can be used to not only find the magnitude of the magnetic flux, but also the direction.

$$\frac{\Omega_P - \Omega_E}{R_e} + \frac{\Omega_P - \Omega_W}{R_w} + \frac{\Omega_P - \Omega_N}{R_n} + \frac{\Omega_P - \Omega_S}{R_s} = 0 \tag{3.10}$$

The benefit of solving this equation, is that it needs less computational power than other finite methods. The MEC method is one of the oldest methods to model magnetic devices. In the regions where you have coils or permanent magnets, the reluctance equation needs to be modified for that region. Coils can be modeled with a magnetomotive force that corresponds to the MMF produced at that given finite region. With a MMF in the x-direction, the following equation is valid [1]:

$$\frac{\Omega_P - \Omega_E - F_e}{R_e} + \frac{\Omega_P - \Omega_W - F_w}{R_w} + \frac{\Omega_P - \Omega_N}{R_n} + \frac{\Omega_P - \Omega_S}{R_s} = 0 \tag{3.11}$$

With uniform mesh, F_e and F_w will have equal magnitude but have opposite signs. The MMF sources are connected in series with the reluctance elements. In a similar way, permanent magnets can be modeled with a flux source parallel to the reluctance elements. The magnitude of the flux source is the product of the remanence (Br) and the finite flux tube area (in 2D analysis it corresponds to the width of the element normal to the flux direction). For PM source in the x-direction, the following equation is valid [1]:

$$\frac{\Omega_P - \Omega_E}{R_e} + \phi_e + \frac{\Omega_P - \Omega_W}{R_w} + \phi_w + \frac{\Omega_P - \Omega_N}{R_n} + \frac{\Omega_P - \Omega_S}{R_s} = 0 \tag{3.12}$$

With a uniform mesh, ϕ_e and ϕ_w will be equal in magnitude but have different signs. The general equation that will describe all effects in the given domain is [1]:

$$\frac{\Omega_P - \Omega_E - F_e}{R_e} + \phi_e + \frac{\Omega_P - \Omega_W - F_w}{R_w} + \phi_w + \frac{\Omega_P - \Omega_N - F_n}{R_n} + \phi_n + \frac{\Omega_P - \Omega_S - F_s}{R_s} + \phi_s = 0 \tag{3.13}$$

It should be pointed out that the remanent fluxes cancel out for the nodes inside the permanent magnet, but contributes at the edges. The remanent flux at one boundary should be calculated as the average of the remanent flux at the two neighboring nodes of the boundary. However the MMF contributes in every element from the current in the neighboring elements normal to the flux direction. For instance, the change in the MMF source in series with the east reluctance from one element to the neighboring element is defined by equation 3.14 [1]

$$Fe_{i,j-1} - Fe_{i,j} = \frac{1}{2}I = \frac{1}{2}J\Delta x\Delta y \tag{3.14}$$

Where the current convection is in the positive z-direction. One can see from this equation that a change in the MMF happens only at the edges of the coil where there is a current density. In the region inside the coil where there is no current density, there is no change in the MMF. However the MMF can change inside if the windings are distributed to create more sinusoidal like MMF.

3.3 Magnetic vector potential

$$\mathbf{B} = \nabla \times \mathbf{A} \tag{3.15}$$

The vector potential (as shown in equation 3.15) is more complex than the scalar potential, but it becomes very simple in 2D [12]. In air it has a very simple analytical solution, given in equation 3.16 [7].

$$\mathbf{A} = \frac{\mu_0}{4\pi}\int_V \frac{\mathbf{J}}{R}dV \tag{3.16}$$

The vector potential in a point has the direction and magnitude determined by the superposition of the surrounding current density vectors, weighted by their distance to the point. In 2D analysis, there exists only current

density vectors in the z-direction. Therefore, there exist only vector potentials in the z-direction (The other two are zero). The vector potential then becomes a scalar potential. From the magnetostatic version of ampere's law:

$$\nabla \times \mathbf{H} = \nabla \times \left[\frac{1}{\mu_0 \mu_r}\mathbf{B}\right] = \nabla \times \left[\frac{1}{\mu_0 \mu_r}\nabla \times \mathbf{A}\right] = \mathbf{J} \tag{3.17}$$

In 2D, equation 3.17 simplifies to the diffusion equation [11]:

$$\frac{\partial}{\partial x}\left[\frac{1}{\mu_0 \mu_r}\frac{\partial A_z}{\partial x}\right] + \frac{\partial}{\partial y}\left[\frac{1}{\mu_0 \mu_r}\frac{\partial A_z}{\partial y}\right] = -J_z \tag{3.18}$$

By assuming constant relative permeability in equation 3.18, poisson's equation is obtained:

$$\frac{\partial^2 A_z}{\partial x^2} + \frac{\partial^2 A_z}{\partial y^2} = -\mu_0 \mu_r J_z \tag{3.19}$$

The vector components of the magnetic flux density is found by the following equations (by the curl the A-field) [11]:

$$B_x = \frac{\partial A_z}{\partial y} - \frac{\partial A_y}{\partial z} \tag{3.20}$$

$$B_y = \frac{\partial A_x}{\partial z} - \frac{\partial A_z}{\partial x} \tag{3.21}$$

$$B_z = \frac{\partial A_y}{\partial x} - \frac{\partial A_x}{\partial y} \tag{3.22}$$

In 2D analysis, the equations are simplified [11]:

$$B_x = \frac{\partial A_z}{\partial y} \tag{3.23}$$

$$B_y = -\frac{\partial A_z}{\partial x} \tag{3.24}$$

A great feature with the magnetic vector potential is that it can be used directly to compute the magnetic flux integral if you apply stokes theorem (see equation 3.25 [11]).

$$\Phi_S = \int_S \nabla \times \mathbf{A} \cdot d\mathbf{S} = \oint_l \mathbf{A} \cdot d\mathbf{l} \tag{3.25}$$

Where the closed line integral path l encloses the surface S. In 2D, the equation 3.25 simplifies to equation 3.26

$$\Phi_{12} = l_z \left[A_z(x1, y1) - A_z(x2, y2)\right] \tag{3.26}$$

where l_z represents the body in the direction normal to the x,y-plane. The line integral becomes zero along the x,y-plane because the magnetic vector potential has zero x,y-components in 2D analysis. For time-dependent FEM analysis, the armature reaction can be accounted for through insertion of the magnetic vector potential into faradays law:

$$\nabla \times \mathbf{E} = -\frac{\nabla \times \partial \mathbf{A}}{\partial t} \tag{3.27}$$

From before we know that the electric field in electrostatics is equal to the negative gradient of the potential. The equation for the electric field in electrodynamics should fulfill both electrostatics plus faradays law. This gives:

$$\mathbf{E} = -\frac{\partial \mathbf{A}}{\partial t} - \nabla V \tag{3.28}$$

The current density used for the time stepping FEM analysis is then:

$$\mathbf{J} = -\sigma \frac{\partial \mathbf{A}}{\partial t} - \sigma \nabla V \tag{3.29}$$

The final equation for the FEM analysis becomes then [2]:

$$\frac{\partial}{\partial x}\left[\nu \frac{\partial A_z}{\partial x}\right] + \frac{\partial}{\partial y}\left[\nu \frac{\partial A_z}{\partial y}\right] = \sigma \left[\frac{\partial A_z}{\partial t} + \frac{\partial V}{\partial z}\right] \tag{3.30}$$

The first source term on the right hand side is the armature reaction, induced currents that try to oppose the change in the magnetic vector potential, thereby the change in the magnetic flux. The second term is the current produced by the applied voltage. The voltage gradient in the z-direction is equal to the negative of the applied voltage over the conductor divided by the length of the conductor. It should be noted that a small mesh in the conductor area makes it possible to simulate the skin effect as well. The left side of the equation is the diffusion equation for the vector potential. The right hand side corresponds to the sources of the diffusion of the vector potential. The diffusion of A is proportional to the reluctivity, which is the inverse of the permeability. Iron has low reluctivity, whereas copper, air and permanent magnets have high reluctivity. The vector potential will diffuse a lot in the direction where the reluctivity is large. This is analogous to that the temperature will diffuse (heat will flow) in the direction where the thermal conductivity is high. For the vector potential, equipotential lines will go in the direction where the reluctivity is small and thereby the magnetic flux density will flow in the lowest reluctivity direction. In opposition to heat flux and electric fields that flows normal to the equipotentials (voltage and temperature), magnetic fields flows along the equipotential lines.

3.4 Finite Modeling of Permanent Magnets

The hysteresis characteristic equation for the permanent magnet can be inserted into amperes law (without displacement currents) and then discretized. This is done to get equation 3.31 [4].

$$\nabla \times [\nu \mathbf{B} - \mathbf{Hc}] = \mathbf{J_{ext}} \tag{3.31}$$

The coercive force of the permanent magnet (excitation) in equation 3.31 can be moved over to the right side of the get equation 3.32.

$$\nabla \times (\nu \mathbf{B}) = \mathbf{J_{ext}} + \nabla \times \mathbf{Hc} \tag{3.32}$$

The equation can also be solved with respect to the magnetization vector [4], as in equation 3.33.

$$\nabla \times (\nu \mathbf{B}) = \mathbf{J_{ext}} + \nabla \times (\nu \mu_0 \mathbf{M}) \tag{3.33}$$

In the same way, it is possible to solve the equation with respect to the magnetic vector potential.

$$\nabla \times (\nu \nabla \times \mathbf{A}) = \mathbf{J_{ext}} + \nabla \times \mathbf{Hc} \tag{3.34}$$

In 2D analysis, there is no excitation from the permanent magnet in the z-direction. The curl of the excitation can then be simplified in two dimensions.

$$\frac{\partial}{\partial x}\left[\nu \frac{\partial A_z}{\partial x}\right] + \frac{\partial}{\partial y}\left[\nu \frac{\partial A_z}{\partial y}\right] = -J_{ext} + \frac{\partial Hc_x}{\partial y} - \frac{\partial Hc_y}{\partial x} \tag{3.35}$$

The only region where there is a coercive force is in the permanent magnet region, but the sources of diffusion applies only at the boundaries of the PM where Hc changes to zero. It is easy to see that the permanent magnet has a current winding equivalent ($Hl = NI$).

3.5 FEM model implementation

In figure 3.1 the implementation of the exciter in FEM is shown. Because of symmetry, it is only needed to simulate for one pole and to use anti periodic conditions at the top and bottom boundary. Anti periodic condition means the flux from the permanent magnet divides equally to the top and the bottom boundary, but that the direction of the flux is opposite. Zero vector potential is defined at the left and right boundaries. Zero potential mean that no magnetic flux crosses those boundaries, since the reluctance of air is high. The phases and the polarity of each set of conductors are also shown. Each conductor set is displaced five mechanical degrees with respect to each other. Five mechanical degrees corresponds to 30 electrical degrees since the number of pole pairs in the exciter is 6. The negative sign for the polarity of phase W and Wd in the implementation means that the phases are phase shifted with U and Ud the given mechanical displacement of 5 and 10 degrees (30 and 60 degrees electrical) plus 180 electrical degrees because of the polarity (See figure 3.1). For the time dependent solution, a rotating mesh interface is made in the middle of the air gap so that the two permanent magnets and the outer stator core can move relative to the rotor. With a rotating exciter, the given time step with rotor and stator symmetrically aligned, corresponds to zero voltage in phase U and maximum positive voltage in phase Wd. This is because on constant mechanical rotation, the maximized flux linkage happens 90 electrical degrees before the maximum voltage. The mesh used for the COMSOL simulation is shown in figure 3.3.

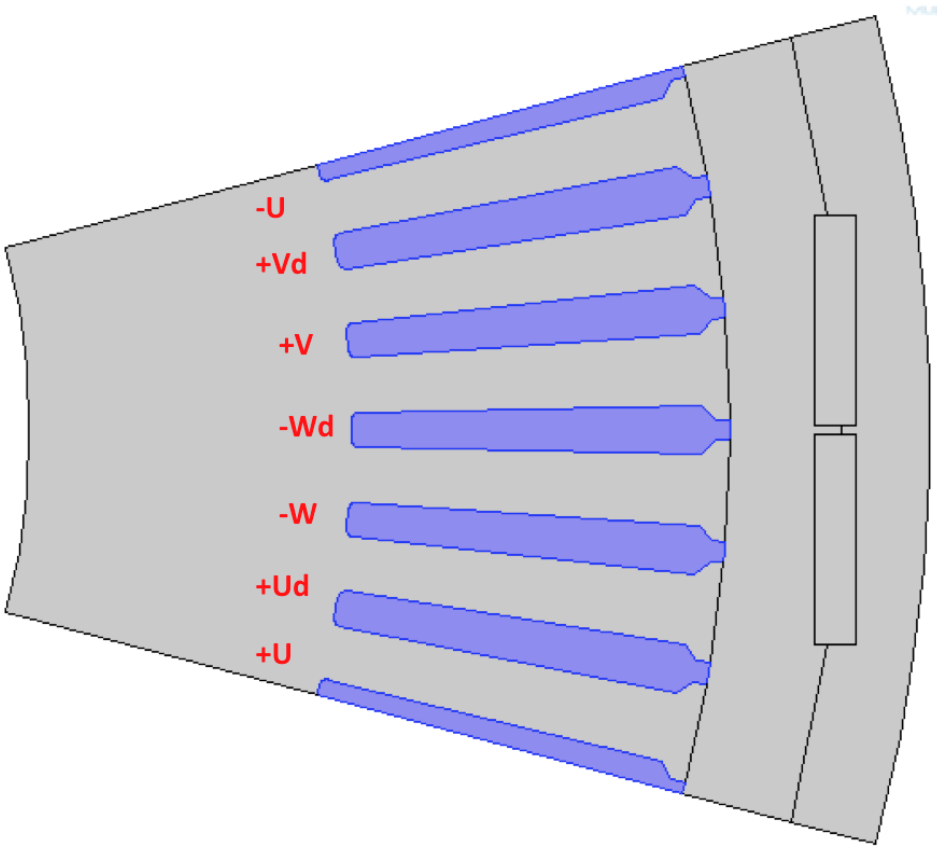

Fig. 3.1 One pole implementation in COMSOL

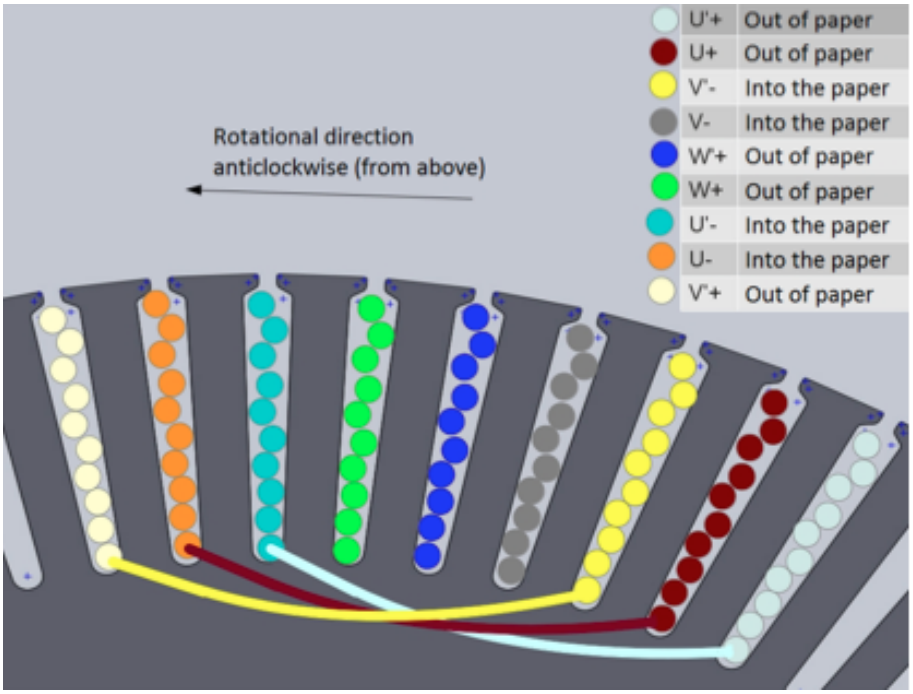

Fig. 3.2 Winding connections for the Exciter

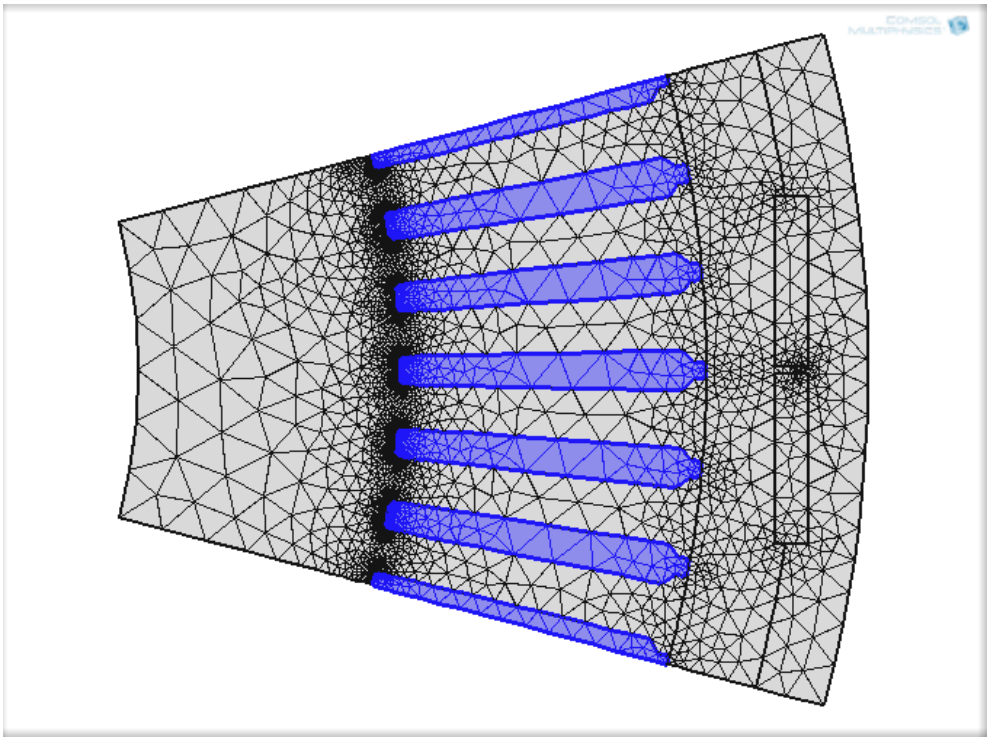

Fig. 3.3 Mesh of the geometry

3.6 FEM inductance calculation

The inductance calculation in FEM is based on the energy method [12]. Current densities are set in the different conductors and the energy of the produced magnetic field is calculated.

$$W_{mag} = l \int \int \frac{1}{2} \mathbf{B} \cdot \mathbf{H} dxdy \tag{3.36}$$

In equation 3.36, l means the length of the 2D geometry in the z direction. The linearized self inductance parameter can be found by modifying equation 3.37 to equation 3.38.

$$W_{mag} = \frac{1}{2} L_{self} I^2 \tag{3.37}$$

$$L_{self} = \frac{2W_{mag}}{I^2} \tag{3.38}$$

The current I in equation 3.37 is the current you put in the winding to find the self inductance for that winding. The FEM calculation should be done for different current levels. It is found that it is hard to get the magnetic material saturated and that the inductance stays the same at different amplitudes of the current. In FEM it is simulated with current amplitudes from 1 to 50 Amperes and there is practically no difference. However, the inductance has a little time dependent variation due to the rotation of the permanent magnets. The time dependent solution can be found by the time stepping method. The mutual inductances between the phases can be found in a similar way, but now current densities should be applied on two phases. The direction of the current densities should be in accordance to the sign convention [12].

$$W_{tot} = \frac{1}{2} L_i I_i^2 + \frac{1}{2} L_j I_j^2 - \frac{1}{2} M_{ij} I_i I_j \tag{3.39}$$

I should be noted that the self inductances has negative signs in the mutual inductance matrix. With the sign convention above, the mutual inductance will be positive if the total magnetic energy is lower than the sum of the magnetic energy from the individual self inductances. The mutual inductance will be negative if the total magnetic energy is higher than the sum of the energy in the individual self inductances. In figure 3.4, 3.5, 3.6, 3.7 and 3.8, the different inductance components for the mutual inductance matrix is given as a function of

time. Indexes are ordered in the way that 1, 2 and 3 corresponds to U, V and W accordingly and that 4, 5 and 6 corresponds to Ud, Vd and Wd accordingly.

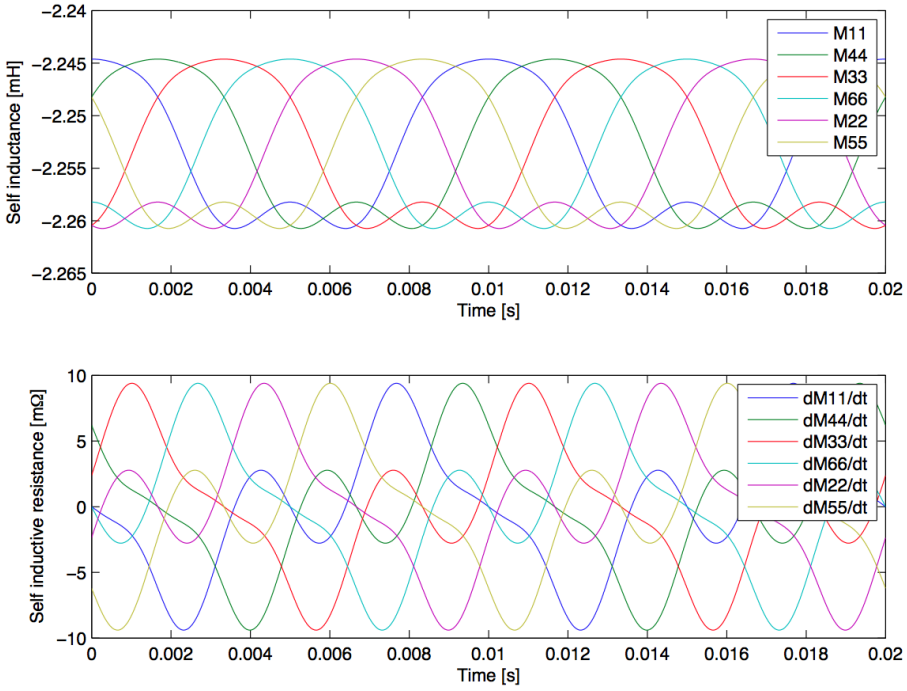

Fig. 3.4 Time dependent self inductances and time dependent derivatives

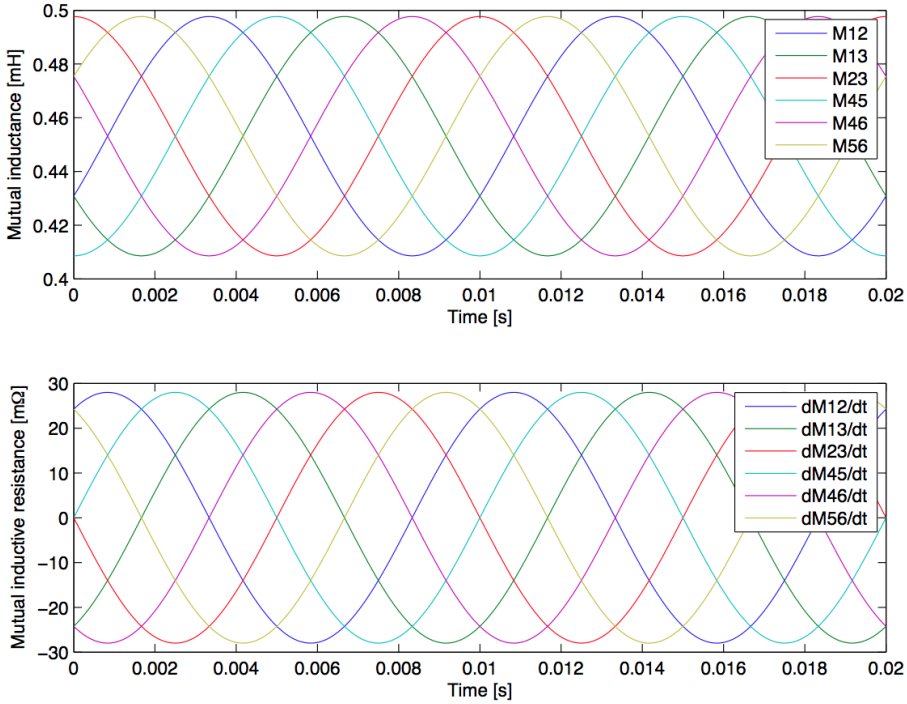

Fig. 3.5 Time dependent mutual inductances and time dependent derivatives

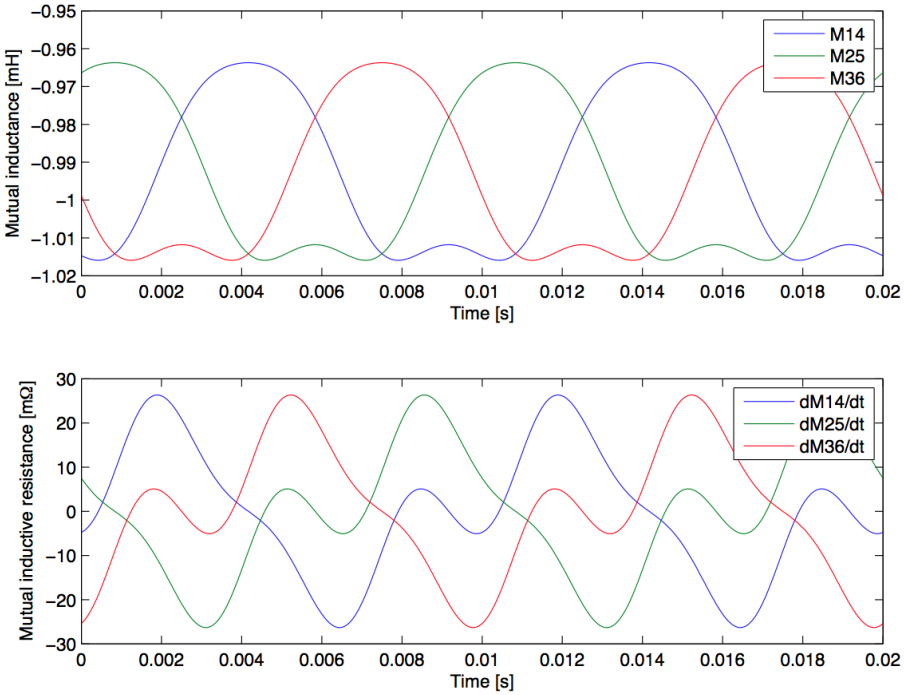

Fig. 3.6 Time dependent mutual inductances and time dependent derivatives

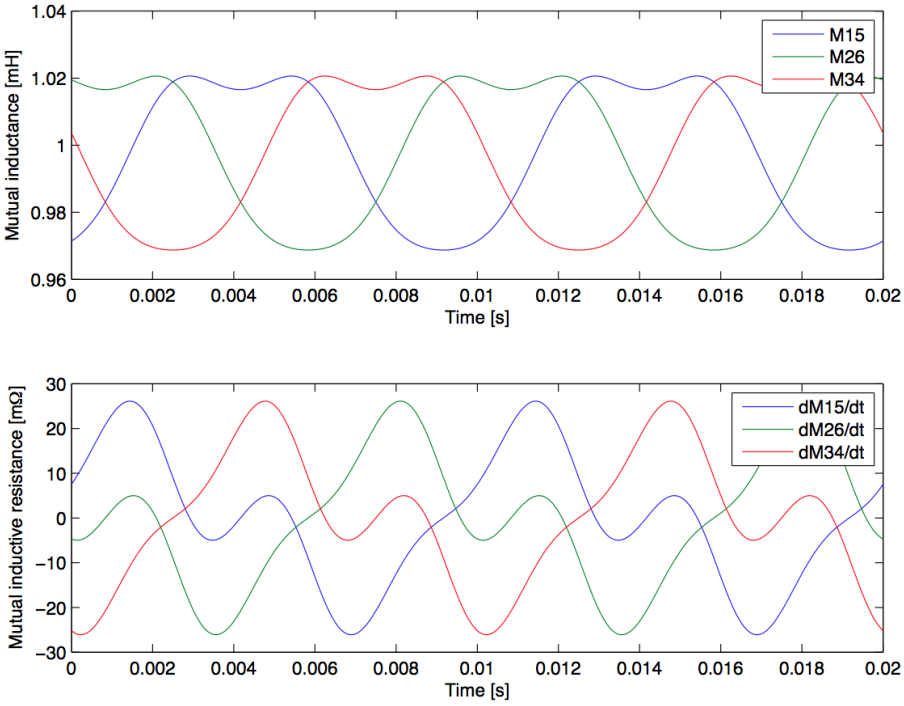

Fig. 3.7 Time dependent mutual inductances and time dependent derivatives

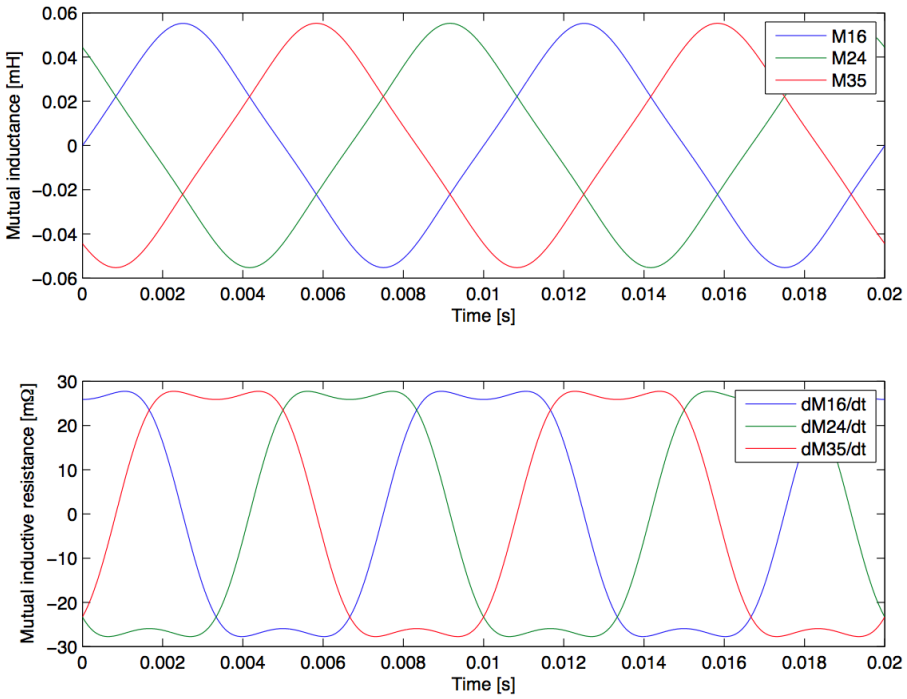

Fig. 3.8 Time dependent mutual inductances and time dependent derivatives

To find the three phase self inductances and mutual inductances, self inductances and mutual inductances of series connected windings needs to be combined to create an equivalent self inductance. Mutual inductances between the windings of the winding pairs also needs to be combined in order to get equivalent mutual inductances as well. A small modification is done in the three phase calculation compared to the six phase calculation by the fact that the length considered for the exciter is 0.1 meter, not 0.2 meter (to be able to operate in the same voltage range). The matrix for the three phase connection is a three times three matrix and the components are defined in figure 3.9 and 3.10.

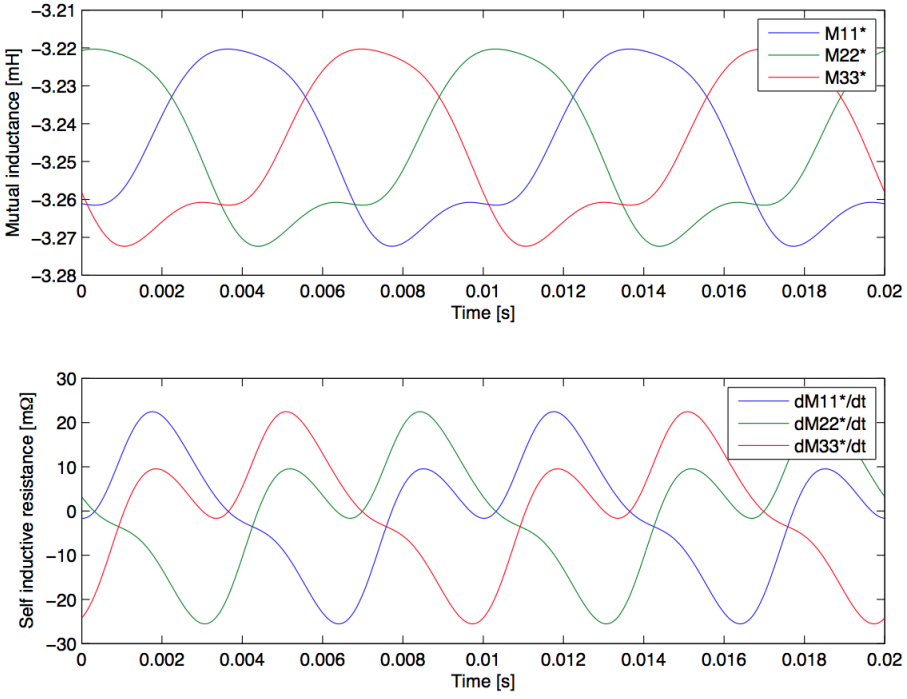

Fig. 3.9 Time dependent self inductances and time dependent derivatives, three phase connection

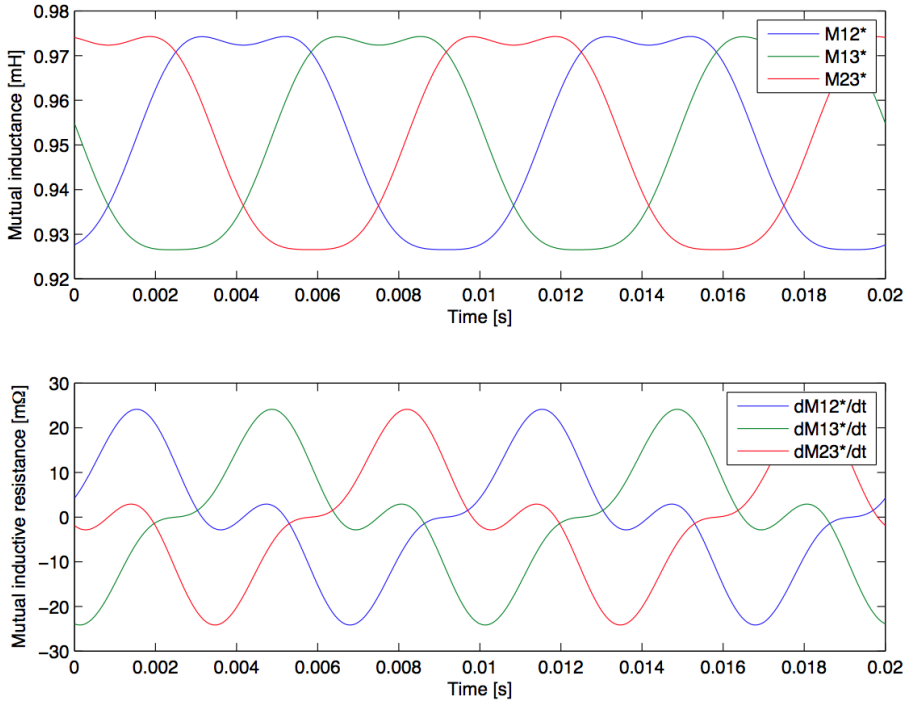

Fig. 3.10 Time dependent mutual inductances and time dependent derivatives, three phase connection

The self inductance of the six phase connection was calculated to be 2.3mH in chapter 2 and this corresponds very well with 2.25mH calculated by FEM, yielding a difference of 2 percent.

3.7 No load voltage calculation

The no load electric field can be calculated at the conductors as minus the change of the magnetic vector potential as the the permanent magnets are rotated with the time stepping method. The total no load voltage can be found by multiplying the electric field with the length in the z-direction. All the conductors of each phase are added together. Since each half of the exciter is parallel connected, it is only needed to add up the voltages for half of the exciter, to get the phase voltages (figure 3.11). The analytical solution for the no-load voltage is found in chapter 5 to 120V and match well with the FEM results which are on average 110V, yielding a difference of 9 percent.

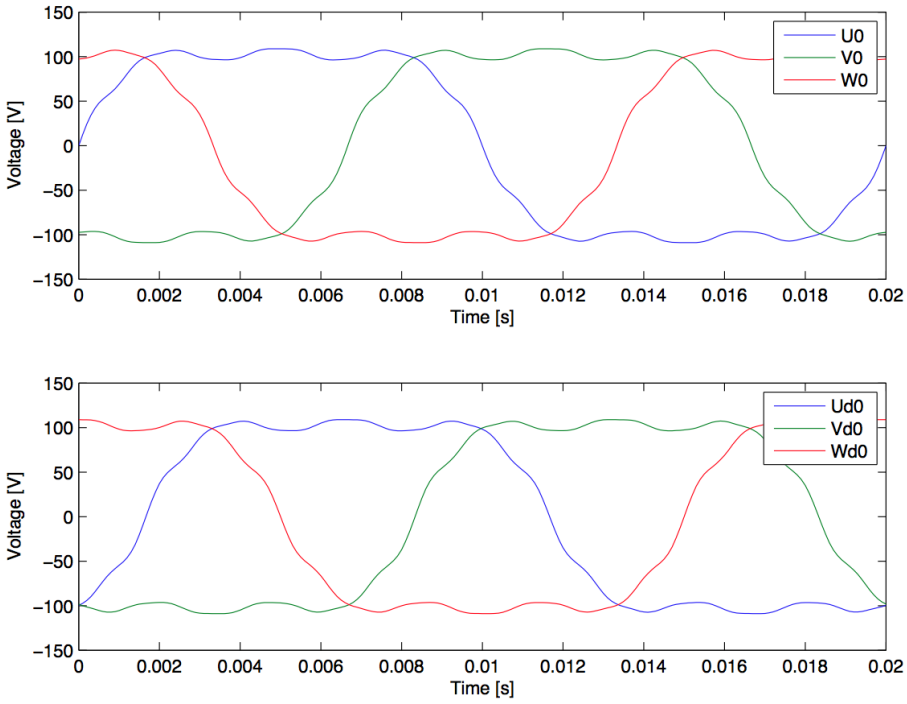

Fig. 3.11 No load phase voltages, six phase

Considering the six phase parallel connection, two and two phases tend to commutate together. It is the pair with the highest absolute value of the line to line voltage, that tend to commutate naturally in a diode rectification bridge. This is shown in figure 3.12.

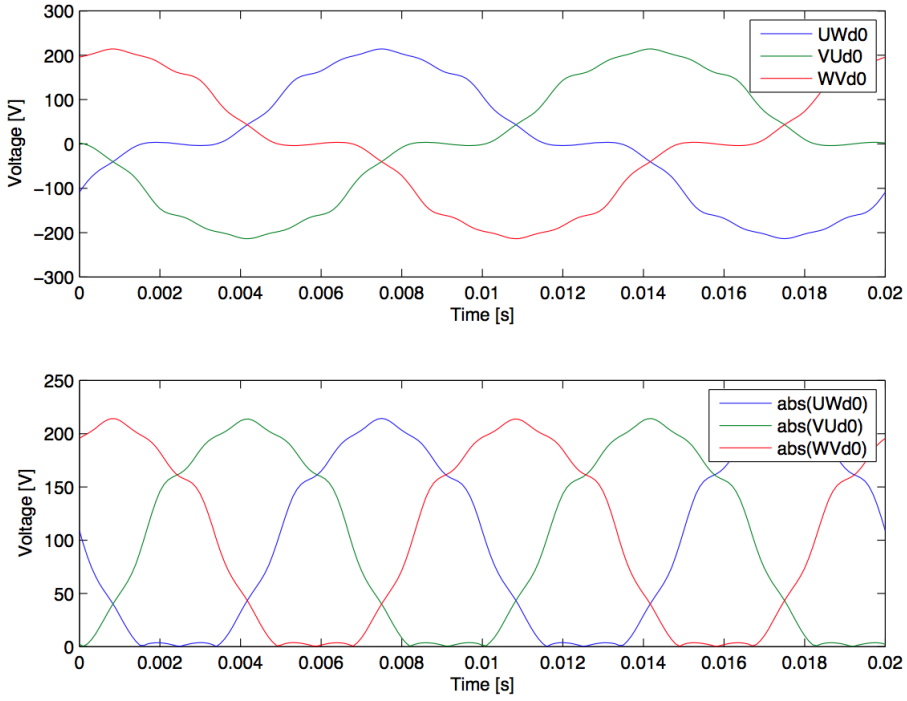

Fig. 3.12 No load line to line voltages, six phase

The three phase voltages (figure 3.13).are calculated as the sum of two and two phases (U and Ud together, V and Vd together and W and Wd together). The difference is that in the three phase connection, the phase voltages are half because the length of the exciter is half.

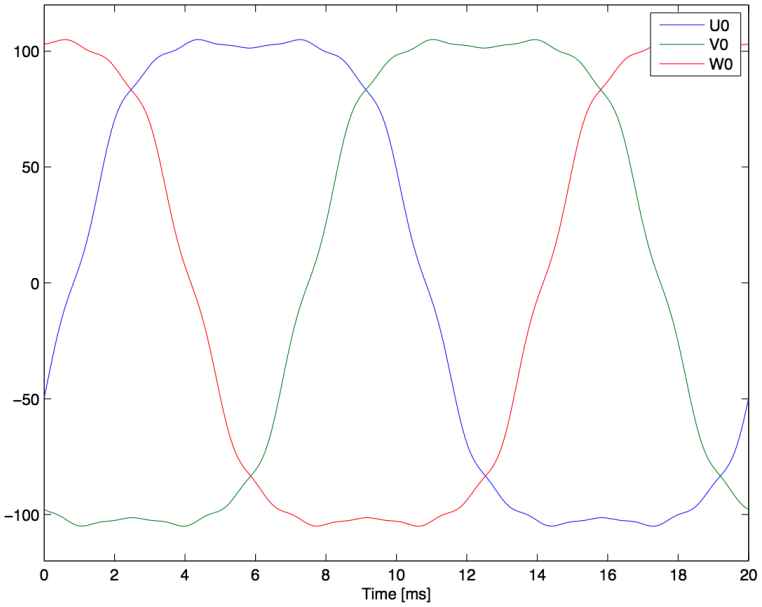

Fig. 3.13 No load voltages, three phase

Chapter 4

Simulation Model

This chapter examines the simulation model in Simulink, used to get out the results in chapter 5. The 6 phase ac system on the rotor should deliver a rectified voltage to supply the rotating electromagnet of the hydroelectric generator with dc current. This can be done in three different ways. First of all, it is possible to connect the six phase voltages into three pairs of phase voltages and to rectify them with a six pulse thyristor rectifier. The voltage of the pairs should be 30 degrees phase shifted with each other in order to get a new balanced three phase system. The other option is to rectify two balanced three phase systems separately and to series connect them on the dc side. The last option is to rectify the six phase system with a twelve pulse thyristor rectifier. The six phase system can be described by vector quantities (assuming sinusoidally distributed windings), as i figure 4.1.

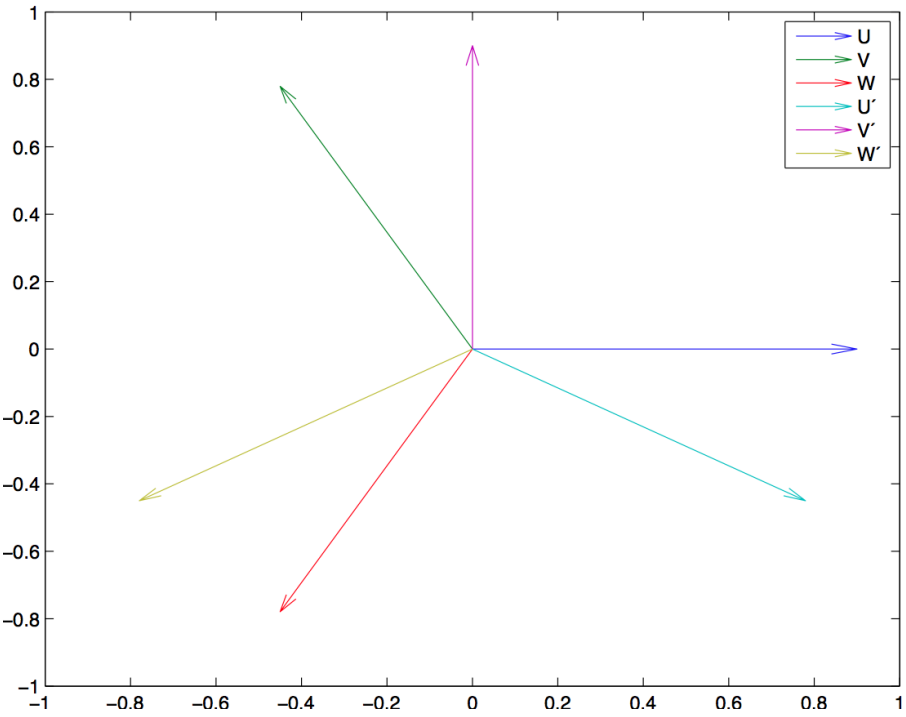

Fig. 4.1 6 phase system vector components

From the FEM calculated time dependent inductance matrix, the terminal voltage can be found. The induced voltage is equal to the negative of the derivate of the flux linkage through the coils of each phase (equation 2.18). The flux contribution from the other phases are found from the inductance matrix [8]. Since this flux contribution should be differentiated, the product rule is used. The major part of the armature reaction is due to the inductance matrix times the derivate of current vector. The minor part of the armature reaction is due to the derivative of the inductance matrix times the current vector. The last part which should be accounted for is the voltage drop due to the parasitic resistance of the coil. That one is measured to be $62.5m\Omega$ (R_s).

$$\begin{bmatrix} U \\ V \\ W \\ Ud \\ Vd \\ Wd \end{bmatrix} = \begin{bmatrix} e_u \\ e_v \\ e_w \\ e_{ud} \\ e_{vd} \\ e_{wd} \end{bmatrix} + \mathbf{v_{ar1}} + \mathbf{v_{ar2}} - R_s \begin{bmatrix} i_u \\ i_v \\ i_w \\ i_{ud} \\ i_{vd} \\ i_{wd} \end{bmatrix} \tag{4.1}$$

$$\mathbf{v_{ar1}} = \begin{bmatrix} M_{11} & M_{12} & M_{13} & M_{14} & M_{15} & M_{16} \\ M_{21} & M_{22} & M_{23} & M_{24} & M_{25} & M_{26} \\ M_{31} & M_{32} & M_{33} & M_{34} & M_{35} & M_{36} \\ M_{41} & M_{42} & M_{43} & M_{44} & M_{45} & M_{46} \\ M_{51} & M_{52} & M_{53} & M_{54} & M_{55} & M_{56} \\ M_{61} & M_{62} & M_{63} & M_{64} & M_{65} & M_{66} \end{bmatrix} \begin{bmatrix} \frac{di_u}{dt} \\ \frac{di_v}{dt} \\ \frac{di_w}{dt} \\ \frac{di_{ud}}{dt} \\ \frac{di_{vd}}{dt} \\ \frac{di_{wd}}{dt} \end{bmatrix} \tag{4.2}$$

$$\mathbf{v_{ar2}} = \begin{bmatrix} \frac{dM_{11}}{dt} & \frac{dM_{12}}{dt} & \frac{M_{13}}{dt} & \frac{M_{14}}{dt} & \frac{M_{15}}{dt} & \frac{dM_{16}}{dt} \\ \frac{dM_{21}}{dt} & \frac{dM_{22}}{dt} & \frac{M_{23}}{dt} & \frac{M_{24}}{dt} & \frac{M_{25}}{dt} & \frac{dM_{26}}{dt} \\ \frac{dM_{31}}{dt} & \frac{dM_{32}}{dt} & \frac{M_{33}}{dt} & \frac{M_{34}}{dt} & \frac{M_{35}}{dt} & \frac{dM_{36}}{dt} \\ \frac{dM_{41}}{dt} & \frac{dM_{42}}{dt} & \frac{M_{43}}{dt} & \frac{M_{44}}{dt} & \frac{M_{45}}{dt} & \frac{dM_{46}}{dt} \\ \frac{dM_{51}}{dt} & \frac{dM_{52}}{dt} & \frac{M_{53}}{dt} & \frac{M_{54}}{dt} & \frac{M_{55}}{dt} & \frac{dM_{56}}{dt} \\ \frac{dM_{61}}{dt} & \frac{dM_{62}}{dt} & \frac{M_{63}}{dt} & \frac{M_{64}}{dt} & \frac{M_{65}}{dt} & \frac{dM_{66}}{dt} \end{bmatrix} \begin{bmatrix} i_u \\ i_v \\ i_w \\ i_{ud} \\ i_{vd} \\ i_{wd} \end{bmatrix} \tag{4.3}$$

For the three phase connection, the armature reaction equation becomes simpler.

$$\begin{bmatrix} U \\ V \\ W \end{bmatrix} = \begin{bmatrix} e_u \\ e_v \\ e_w \end{bmatrix} + \begin{bmatrix} M_{11}^* & M_{12}^* & M_{13}^* \\ M_{21}^* & M_{22}^* & M_{23}^* \\ M_{31}^* & M_{32}^* & M_{33}^* \end{bmatrix} \begin{bmatrix} \frac{di_u}{dt} \\ \frac{di_v}{dt} \\ \frac{di_w}{dt} \end{bmatrix} + \begin{bmatrix} \frac{dM_{11}^*}{dt} & \frac{dM_{12}^*}{dt} & \frac{M_{13}^*}{dt} \\ \frac{dM_{21}^*}{dt} & \frac{dM_{22}^*}{dt} & \frac{M_{23}^*}{dt} \\ \frac{dM_{31}^*}{dt} & \frac{dM_{32}^*}{dt} & \frac{M_{33}^*}{dt} \end{bmatrix} \begin{bmatrix} i_u \\ i_v \\ i_w \end{bmatrix} - R_s \begin{bmatrix} i_u \\ i_v \\ i_w \end{bmatrix} \tag{4.4}$$

4.1 Three phase connection

Figure 4.3 shows the generalized circuit for simulation in Simulink for the three phase connection. The generalization is made from the true circuit in figure 4.2. The load circuit has a resistance (R_{load} 3 Ω and an inductance of 0.53H. Two and two pairs of phases conducts the load current normally, but during the commutation, all phases conducts.The armature reaction for negative and positive current commutation is symmetrical. The generalized voltages represents different phase voltages for different intervals. When commutation does not occur anymore, the voltage v_j is removed from the circuit. This means that the j index is not active as well as the commutation integrator is not active.

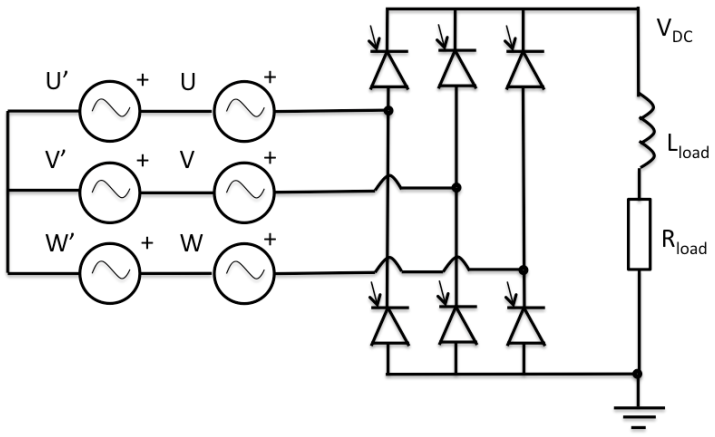

Fig. 4.2 Circuit diagram for the Three Phase connection

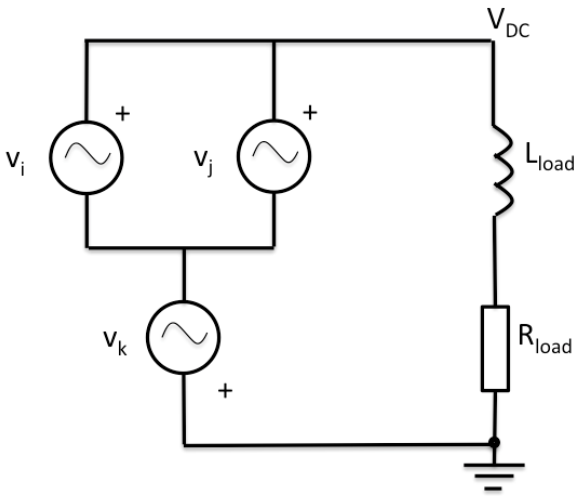

Fig. 4.3 Generalized simulation circuit

Each index in the circuit is associated with a specific no load voltage and a specific position in the inductance matrix for every interval of 60 degrees. Table 4.1 shows the connection between the indexes and the phases for different intervals and the corresponding equations are as follows.

$$v_i = e_i + M_{ii}\frac{di_i}{dt} + M_{ij}\frac{di_j}{dt} + M_{ik}\frac{di_k}{dt} + (\frac{dM_{ii}}{dt} - R_s)i_i + \frac{dM_{ij}}{dt}i_j + \frac{dM_{ik}}{dt}i_k. \tag{4.5}$$

$$v_j = e_j + M_{ji}\frac{di_i}{dt} + M_{jj}\frac{di_j}{dt} + M_{jk}\frac{di_k}{dt} + \frac{dM_{ji}}{dt}i_i + (\frac{dM_{jj}}{dt} - R_s)i_j + \frac{dM_{jk}}{dt}i_k \tag{4.6}$$

$$v_k = e_k + M_{ki}\frac{di_i}{dt} + M_{kj}\frac{di_j}{dt} + M_{kk}\frac{di_k}{dt} + \frac{dM_{ki}}{dt}i_i + \frac{dM_{kj}}{dt}i_j + (\frac{dM_{kk}}{dt} - R_s)i_k \tag{4.7}$$

where v_i, v_j and v_k is source voltage, e_i, e_j and e_k is the no load source voltage and R_s is the internal resistance of the phase coils. By applying Kirchoffs voltage law, equation 4.8 is found.

$$v_i - v_k = R_{load}i_{load} + L_{load}\frac{di_{load}}{dt} \tag{4.8}$$

Insertion of equation 4.5 and 4.7 into equation 4.8 gives

$$e_i - e_k + L_i\frac{di_i}{dt} + L_j\frac{di_j}{dt} + L_k\frac{di_k}{dt} + R_ii_i + R_ji_j + R_ki_k = R_{load}i_{load} + L_{load}\frac{di_{load}}{dt} \tag{4.9}$$

where $L_i = M_{ii} - M_{ki}$, $L_j = M_{ij} - M_{kj}$, $L_k = M_{ik} - M_{kk}$, $R_i = \frac{dM_{ii}}{dt} - \frac{dM_{ki}}{dt} - R_s$, $R_j = \frac{dM_{ij}}{dt} - \frac{dM_{kj}}{dt}$ and $R_k = \frac{dM_{ik}}{dt} - \frac{dM_{kk}}{dt} + R_s$. From Kirchoffs current law, it can be shown that $i_i = i_{load} - i_{com}$, $i_j = i_{com}$ and $i_k = -i_{load}$. Insertion gives

$$e_i - e_k + (L_j - L_i)\frac{di_{com}}{dt} + (R_j - R_i)i_{com} = (R_{load} + R_k - R_i)i_{load} + (L_{load} + L_k - L_i)\frac{di_{load}}{dt} \tag{4.10}$$

Kirchoffs voltage law also gives

$$v_j - v_i = 0 \tag{4.11}$$

The armature reaction can be inserted into equation 4.11, yielding

$$e_j - e_i + L_i^*\frac{di_i}{dt} + L_j^*\frac{di_j}{dt} + L_k^*\frac{di_k}{dt} + R_i^*i_i + R_j^*i_j + R_k^*i_k = 0 \tag{4.12}$$

Where $L_i^* = M_{ji} - M_{ii}$, $L_j^* = M_{jj} - M_{ij}$, $L_k^* = M_{jk} - M_{ik}$, $R_i^* = \frac{dM_{ji}}{dt} - \frac{dM_{ii}}{dt} + R_s$, $R_j^* = \frac{dM_{jj}}{dt} - \frac{dM_{ij}}{dt} - R_s$ and $R_k^* = \frac{dM_{jk}}{dt} - \frac{dM_{ik}}{dt}$. By applying Kirchoff current law, equation 4.12 is modified to

$$e_j - e_i + (R_i^* - R_k^*)i_{load} + (L_i^* - L_k^*)\frac{di_{load}}{dt} = (R_i^* - R_j^*)i_{com} + (L_i^* - L_j^*)\frac{di_{com}}{dt} \tag{4.13}$$

Equation 4.10 and equation 4.13 forms together two generalized coupled differential equations.

$$v_{main} = R_{main} i_{load} + L_{main} \frac{di_{load}}{dt} \tag{4.14}$$

$$v_{com} = R_{com} i_{com} + L_{com} \frac{di_{com}}{dt} \tag{4.15}$$

The states (load current and commutation current) in equation 4.14 and 4.15 can be solved by Laplace transformation in the simulink solver, yielding

$$i_{load} = \frac{v_{main}}{R_{main} + sL_{main}} \tag{4.16}$$

$$i_{com} = \frac{v_{com}}{R_{com} + sL_{com}} \tag{4.17}$$

where $L_{main} = L_{load} + L_k - L_i$, $R_{main} = R_{load} + R_k - R_i$, $L_{com} = L_i^* - L_k^*$ and $R_{com} = R_i^* - R_k^*$, $v_{main} = e_i - e_k + (L_j - L_i)\frac{di_{com}}{dt} + (R_j - R_i)i_{com}$ and $v_{com} = e_j - e_i + (R_i^* - R_k^*)i_{load} + (L_i^* - L_k^*)\frac{di_{load}}{dt}$. Given constant parameters are: $R_{load} = 3\Omega$, $L_{load} = 0.53H$ and $R_s = 0.0625\Omega$.

Table 4.1 Associated voltages and indexes for different intervals

Firing angle	e_i	e_j	e_k
45+α	U	W	V
105+α	-W	-V	-U
165+α	V	U	W
225+α	-U	-W	-V
285+α	W	V	U
345+α	-V	-U	-W

4.2 Six phase connection

Figure 4.5 shows the general simulation circuit for the six phase connection (derived from the main circuit in figure 4.4. The commutation circuit is a result of the fact that in the six phase system, the commutation happens in two phases at the same time. There are six phases, but only four phases are active during each commutation. When there is no commutation, the j index and the l index are not active, as well as the commutation integrator is not active.

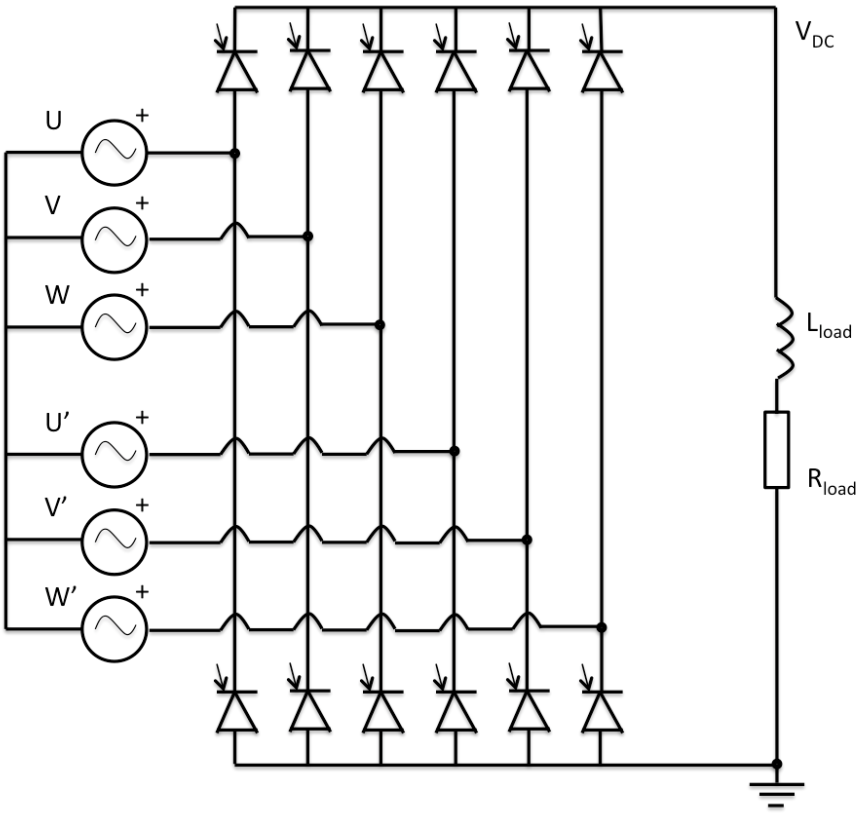

Fig. 4.4 Circuit diagram for the Parallel connection

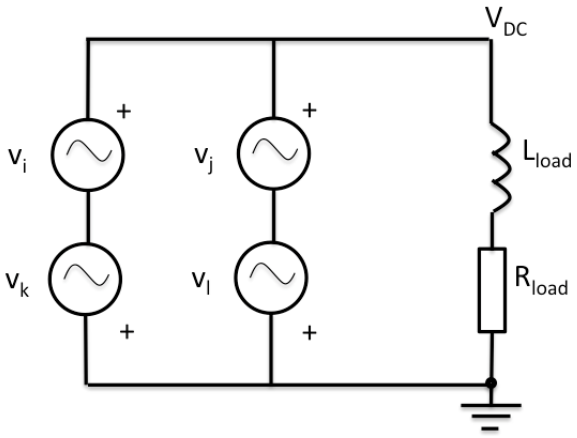

Fig. 4.5 Generalized simulation circuit

The simulation model for the six phase system can be derived the same way as in the three phase connection. The interval table is found in table 4.2 and the equations are

$$v_i = e_i + M_{ii}\frac{di_i}{dt} + M_{ij}\frac{di_j}{dt} + M_{ik}\frac{di_k}{dt} + M_{il}\frac{di_l}{dt} + (\frac{dM_{ii}}{dt} - R_s)i_i + \frac{dM_{ij}}{dt}i_j + \frac{dM_{ik}}{dt}i_k + \frac{dM_{il}}{dt}i_l \quad (4.18)$$

$$v_j = e_j + M_{ji}\frac{di_i}{dt} + M_{jj}\frac{di_j}{dt} + M_{jk}\frac{di_k}{dt} + M_{jl}\frac{di_l}{dt} + \frac{dM_{ji}}{dt}i_i + (\frac{dM_{jj}}{dt} - R_s)i_j + \frac{dM_{jk}}{dt}i_k + \frac{dM_{jl}}{dt}i_l \quad (4.19)$$

$$v_k = e_k + M_{ki}\frac{di_i}{dt} + M_{kj}\frac{di_j}{dt} + M_{kk}\frac{di_k}{dt} + M_{kl}\frac{di_l}{dt} + \frac{dM_{ki}}{dt}i_i + \frac{dM_{kj}}{dt}i_j + (\frac{dM_{kk}}{dt} - R_s)i_k + \frac{dM_{kl}}{dt}i_l \quad (4.20)$$

$$v_l = e_l + M_{li}\frac{di_i}{dt} + M_{lj}\frac{di_j}{dt} + M_{lk}\frac{di_k}{dt} + M_{ll}\frac{di_l}{dt} + \frac{dM_{li}}{dt}i_i + \frac{dM_{lj}}{dt}i_j + \frac{dM_{lk}}{dt}i_k + (\frac{dM_{ll}}{dt} - R_s)i_l \quad (4.21)$$

First KVL loop forms the following equation

$$v_i - v_k = R_{load}i_{load} + L_{load}\frac{di_{load}}{dt} \quad (4.22)$$

Equation 4.18 and 4.20 can be inserted into equation 4.22 to get

$$e_i - e_k + L_i\frac{di_i}{dt} + L_j\frac{di_j}{dt} + L_k\frac{di_k}{dt} + L_l\frac{di_l}{dt} + R_ii_i + R_ji_j + R_ki_k + R_li_l = R_{load}i_{load} + L_{load}\frac{di_{load}}{dt} \quad (4.23)$$

where $L_i = M_{ii} - M_{ki}$, $L_j = M_{ij} - M_{kj}$, $L_k = M_{ik} - M_{kk}$, $L_l = M_{il} - M_{kl}$, $R_i = \frac{dM_{ii}}{dt} - \frac{dM_{ki}}{dt} - R_s$, $R_j = \frac{dM_{ij}}{dt} - \frac{dM_{kj}}{dt}$, $R_k = \frac{dM_{ik}}{dt} - \frac{dM_{kk}}{dt} + R_s$ and $R_l = \frac{dM_{il}}{dt} - \frac{dM_{kl}}{dt}$. From Kirchoff's current law, it can be shown that $i_i = i_{load} - i_{com}$, $i_j = i_{com}$, $i_k = -i_{load} + i_{com}$ and $i_l = -i_{com}$. Considering Kirchoff's current law, equation 4.23 is simplifyed to

$$e_i - e_k + (L_j - L_i + L_l - L_k)\frac{di_{com}}{dt} + (R_j - R_i + R_l - R_k)i_{com} = (R_{load} + R_k - R_i)i_{load} + (L_{load} + L_k - L_i)\frac{di_{load}}{dt} \quad (4.24)$$

Another KVL loop yields

$$v_j - v_l + v_k - v_i = 0 \quad (4.25)$$

The same type of insertion method can be used to obtain

$$e_j - e_l + e_k - e_i + L_i^*\frac{di_i}{dt} + L_j^*\frac{di_j}{dt} + L_k^*\frac{di_k}{dt} + L_l^*\frac{di_l}{dt} + R_i^*i_i + R_j^*i_j + R_k^*i_k + R_l^*i_l = 0 \quad (4.26)$$

where $L_i^* = M_{ji} - M_{li} + M_{ki} - M_{ii}$, $L_j^* = M_{jj} - M_{lj} + M_{kj} - M_{ij}$, $L_k^* = M_{jk} - M_{lk} + M_{kk} - M_{ik}$, $L_l^* = M_{jl} - M_{ll} + M_{kl} - M_{il}$, $R_i^* = \frac{dM_{ji}}{dt} - \frac{dM_{li}}{dt} + \frac{dM_{ki}}{dt} - \frac{dM_{ii}}{dt} + R_s$, $R_j^* = \frac{dM_{jj}}{dt} - \frac{dM_{lj}}{dt} + \frac{dM_{kj}}{dt} - \frac{dM_{ij}}{dt} - R_s$, $R_k^* = \frac{dM_{jk}}{dt} - \frac{dM_{lk}}{dt} + \frac{dM_{kk}}{dt} - \frac{dM_{ik}}{dt} - R_s$ and $R_l^* = \frac{dM_{jl}}{dt} - \frac{dM_{ll}}{dt} + \frac{dM_{kl}}{dt} - \frac{dM_{il}}{dt} + R_s$. Further simplification by introducing i_{load} and i_{com} gives

$$e_j - e_l + e_k - e_i + (R_i^* - R_k^*)i_{load} + (L_i^* - L_k^*)\frac{di_{load}}{dt} = (R_i^* - R_j^* + R_k^* - R_l^*)i_{com} + (L_i^* - L_j^* + L_k^* - L_l^*)\frac{di_{com}}{dt} \quad (4.27)$$

The same type of coupled integrator differential equation system is obtained for the six phase system as well (See equation 4.28 and 4.29), but the parameters are modified.

$$i_{load} = \frac{v_{main}}{R_{main} + sL_{main}} \quad (4.28)$$

$$i_{com} = \frac{v_{com}}{R_{com} + sL_{com}} \quad (4.29)$$

where $L_{main} = L_{load} + L_k - L_i$, $R_{main} = R_{load} + R_k - R_i$, $L_{com} = L_i^* - L_j^* + L_k^* - L_l^*$ and $R_{com} = R_i^* - R_j^* + R_k^* - R_l^*$, $v_{main} = e_i - e_k + (L_j - L_i + L_l - L_k)\frac{di_{com}}{dt} + (R_j - R_i + R_l - R_k)i_{com}$ and $v_{com} = e_j - e_l + e_k - e_i + (R_i^* - R_k^*)i_{load} + (L_i^* - L_k^*)\frac{di_{load}}{dt}$. Given constant parameters is: $R_{load} = 3\Omega$, $L_{load} = 0.53H$ and $R_s = 0.0625\Omega$.

Table 4.2 Associated voltages and indexes for different intervals

Firing angle	e_i	e_j	e_k	e_l
45+α	Ud	W	V	Vd
105+α	U	Ud	Wd	V
165+α	Vd	U	W	Wd
225+α	V	Vd	Ud	W
285+α	Wd	V	U	Ud
345+α	W	Wd	Vd	U

4.3 Double three phase series connection

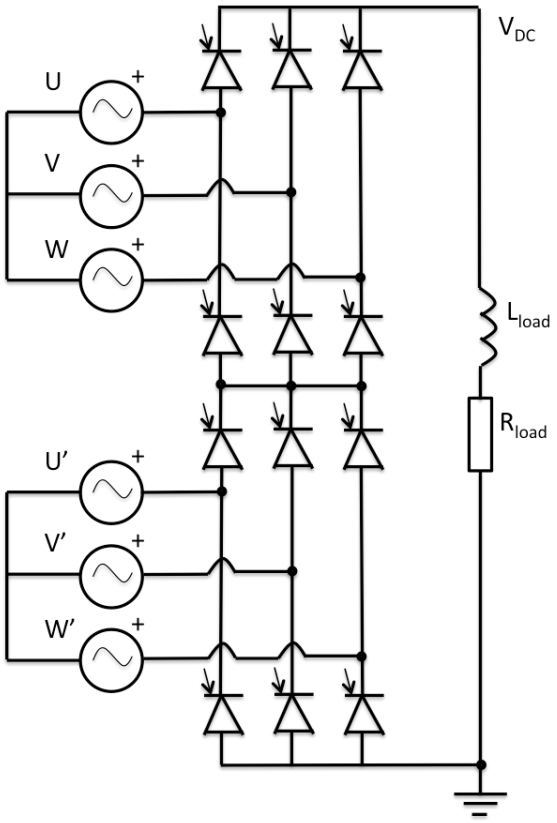

Fig. 4.6 Circuit diagram for the double three phase series connection

For the double three phase series connection, it is possible to have two commutation processes at the same time and also to have different firing angles at the upper and the lower bridge. This makes the simulation model very complex. The armature reaction is also more complex because the commutation of one bridge is dependent on the polarity of the commutation in the other bridge. A model was made with the assumption of same firing angles on both bridges and that the commutations does not overlap. Because of too high inductances in the matrix, the simulation was shown to fail because the commutation did indeed overlap.

Chapter 5

Results

This chapter will begin with the analytical magnetic circuit results and continue further with the simulation results. All simulations are done in Simulink with the time-dependent self and mutual inductances and the no load voltages as input data (calculated from FEM). The model developed in chapter 4 is used and with post processing in Matlab, all the data has been calculated. The post processing starts by converting load current and commutation current to actual phase currents. The same is done for the derivative of the currents. Then the phase currents and the derivative of the phase currents is used to calculated the terminal voltage when the armature reaction is accounted for. Phase voltages and phase currents are multiplied with each other to get the instantaneous phase powers. The phase powers are used to predict the torque ripple. Full load refers to a delay angle of 10 degrees. The angle should not be lower because some commutation voltage is needed from the start to be able to fire the thyristors.

5.1 Analytical results

Analytical results as shown below are calculated from the theory developed in chapter 2. The calculated induced phase voltage should be regarded as no-load amplitude, as the design was optimized for that given voltage. In the three phase machine, the exciter is half in height and the phase voltage will be half of the calculated one in this section.

Average air gap length	l_g	14mm
Air gap width	W_g	30mm
Air gap reluctance	R_g	1856808 $\frac{A}{Wb}$
Air gap permeance	P_g	0.539 $\frac{\mu Wb}{A}$
Flux leakage factor	K_l	0.75
Total flux	ϕ	3.16 mWb
Leakage flux	ϕ_l	0.789 mWb
Air gap flux	ϕ_g	2.37 mWb
Air gap flux density	B_g	0.39T
Rotor speed	n_{mech}	1000 rpm
Pole pairs	n_p	6
Frequency	f	50 Hz
Rotor radius	R	0.2m
Induced electric field	E	4.14 $\frac{V}{m}$
Number of turns per phase, per half pole	N_w	12
Number series connected coils	N_s	6
Induced phase voltage	u	120 V

5.2 Three phase simulation results

The voltage in figure 5.1 shows the difference in the terminal voltage for full load and no load conditions. The reaction is symmetrical for all three phases.

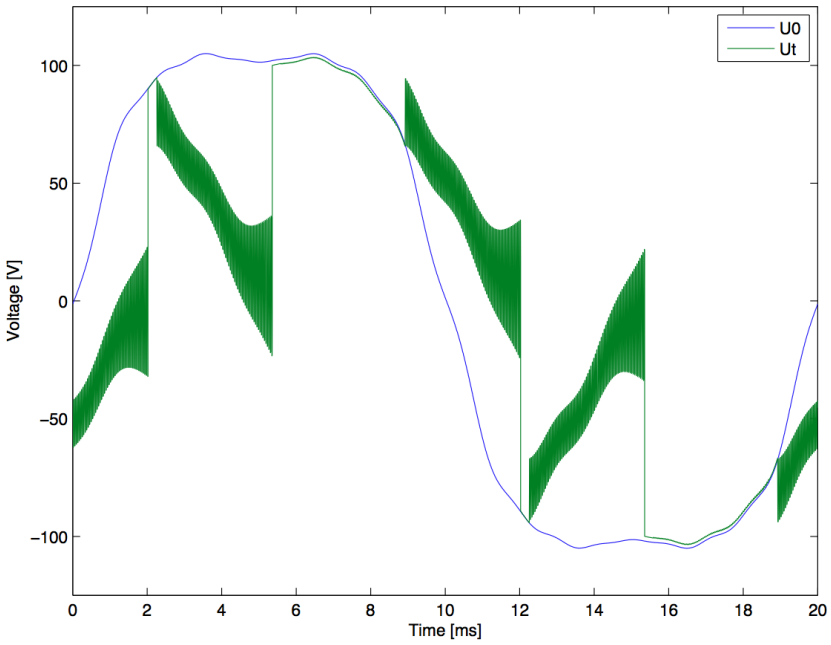

Fig. 5.1 U phase voltage, no load and full load

In the direct current side of the exciter, reactive power does not exist. Figure 5.2 shows how the phase current and phase voltage are phase shifted on the alternating current side of the exciter. This results in reactive power consumption. The reactive power is accumulated in the magnetic field during the commutation process.

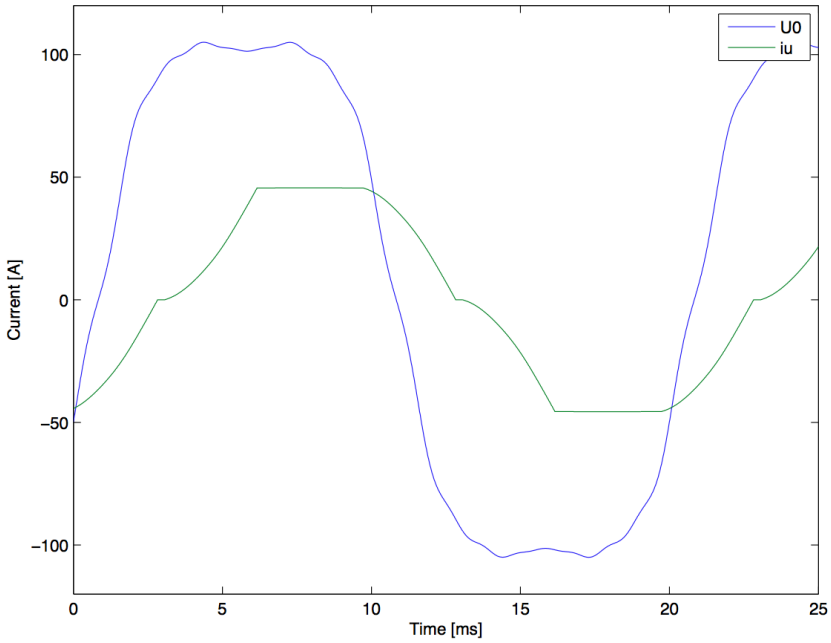

Fig. 5.2 Delay plot, no load phase voltage and full load phase current

Figure 5.3 shows that the phase currents are symmetrically shifted. The figure also shows that commutation occurs nearly all the time since neither of the phases has zero current for a very long time.

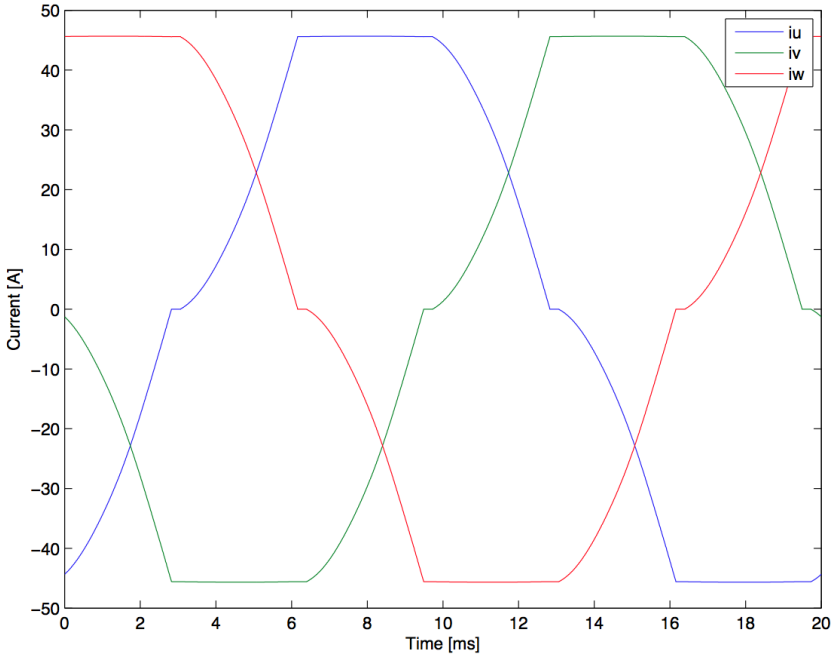

Fig. 5.3 Phase currents

The power absorbed by each phase is very time varying. This is shown in figure 5.4. The net power generated by the exciter is the sum of all the three powers generated. The total instantaneous power generated by the exciter is the source of the torque that the exciter produces. This ripple is plotted in figure 5.5

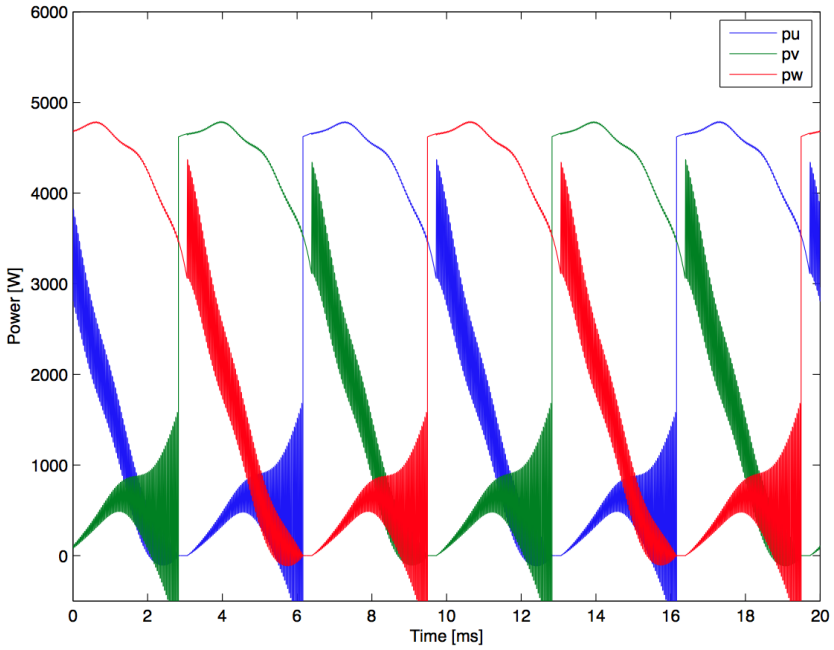

Fig. 5.4 Instantaneous power for each phase

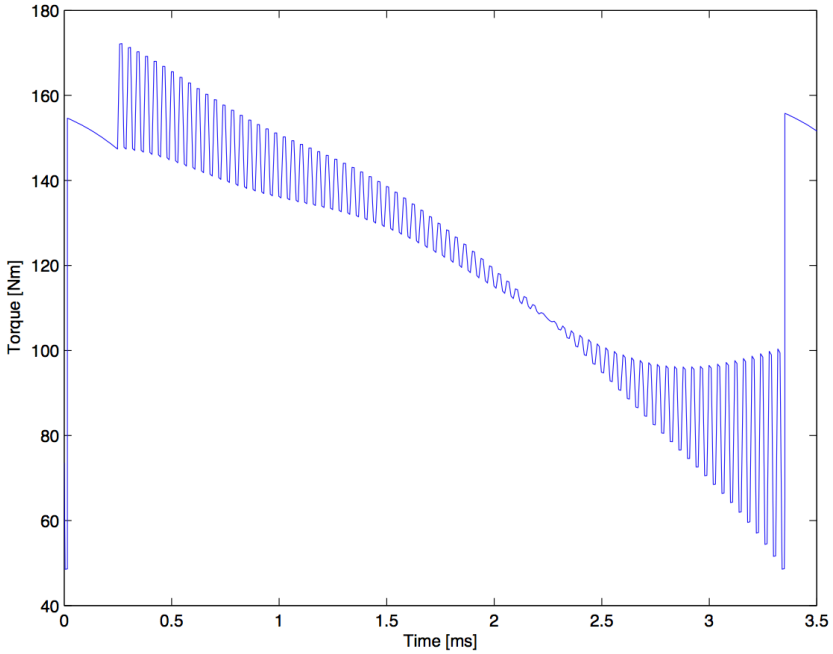

Fig. 5.5 Instantaneous torque variation, full load

5.3 Six phase simulation results

Figure 5.6 and 5.7 shows that the armature reaction for the dotted and the non-dotted phases are different. This is because the phase shift between the phase current and the phase voltage are different for the dotted and the non-dotted (See figure 5.8 and 5.9). This again results in different waveforms for the phase powers shown in figure 5.11 and 5.12. However, the waveforms for the power of the dotted phases are equal but phase shifted and same for the non-dotted phases. The individual phase currents are shown in figure 5.10. The phase currents are symmetrical to each other in order to make the load current stiff.

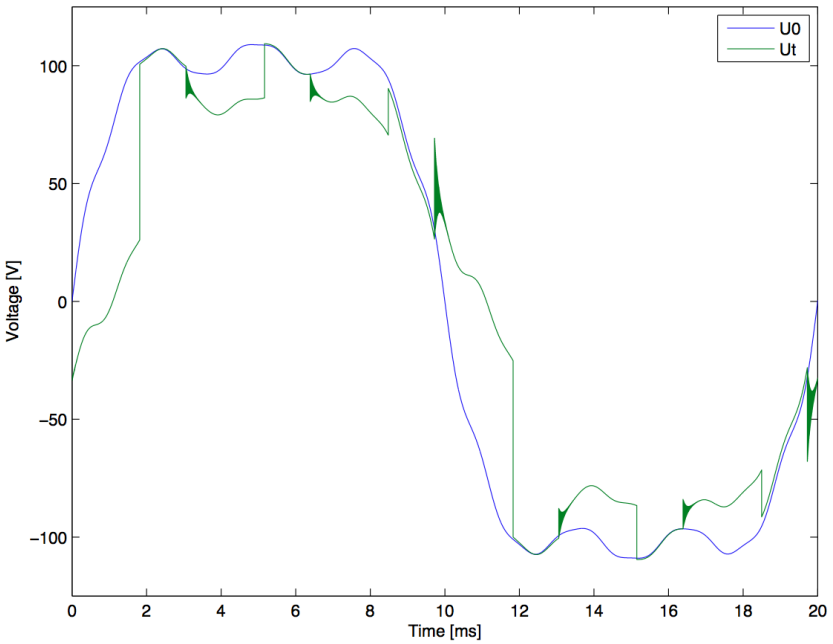

Fig. 5.6 U phase voltage, no load and full load

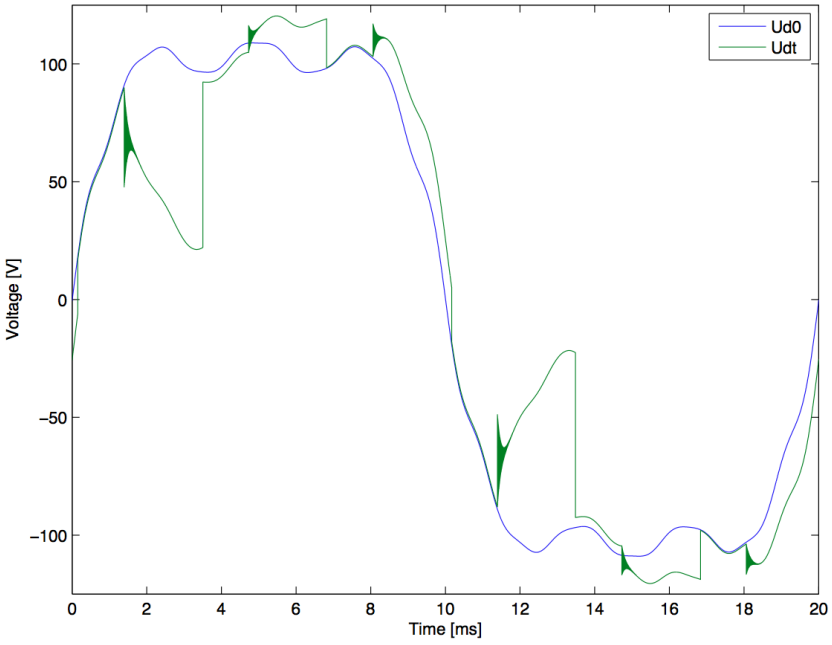

Fig. 5.7 Ud phase voltage, no load and full load

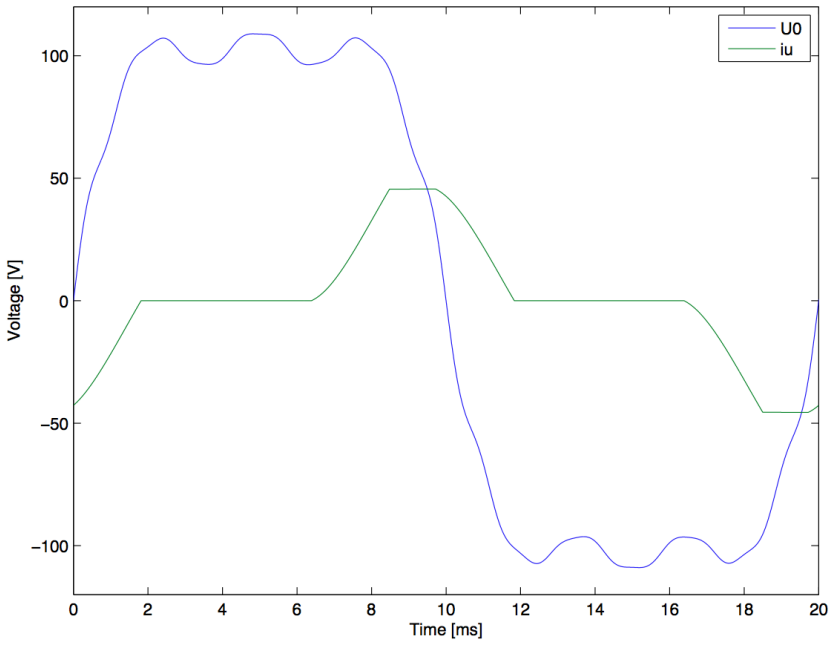

Fig. 5.8 Delay plot U phase, no load phase voltage and full load phase current

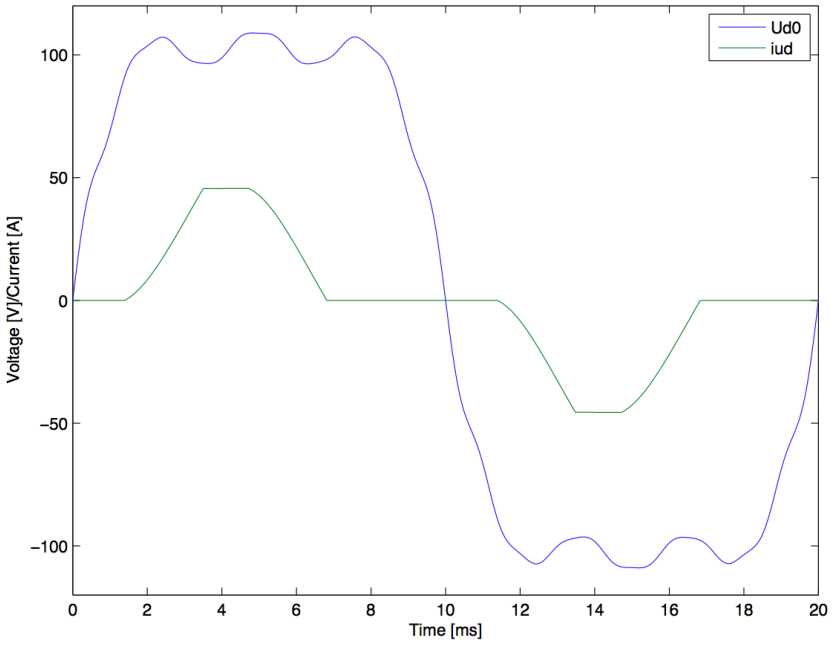

Fig. 5.9 Delay plot Ud phase, no load phase voltage and full load phase current

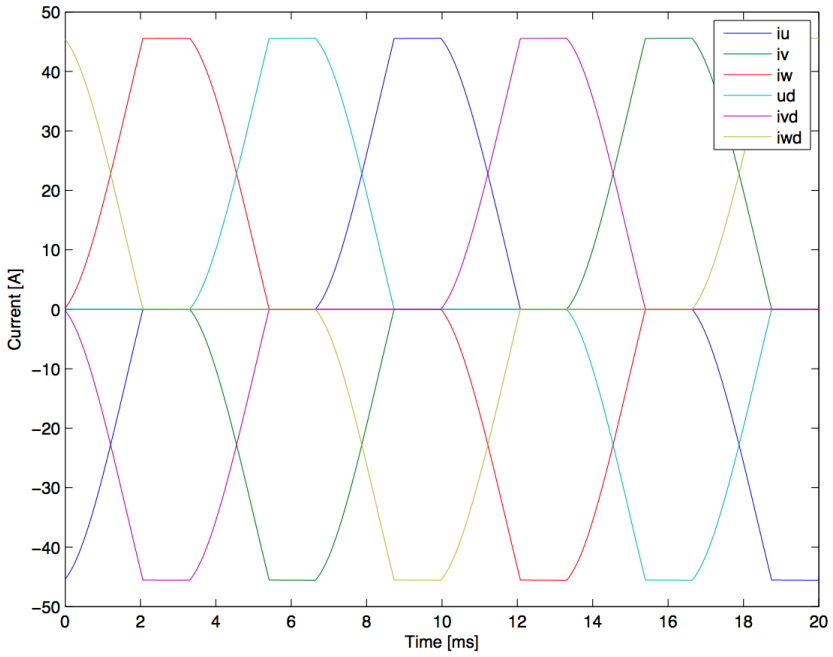

Fig. 5.10 Phase currents

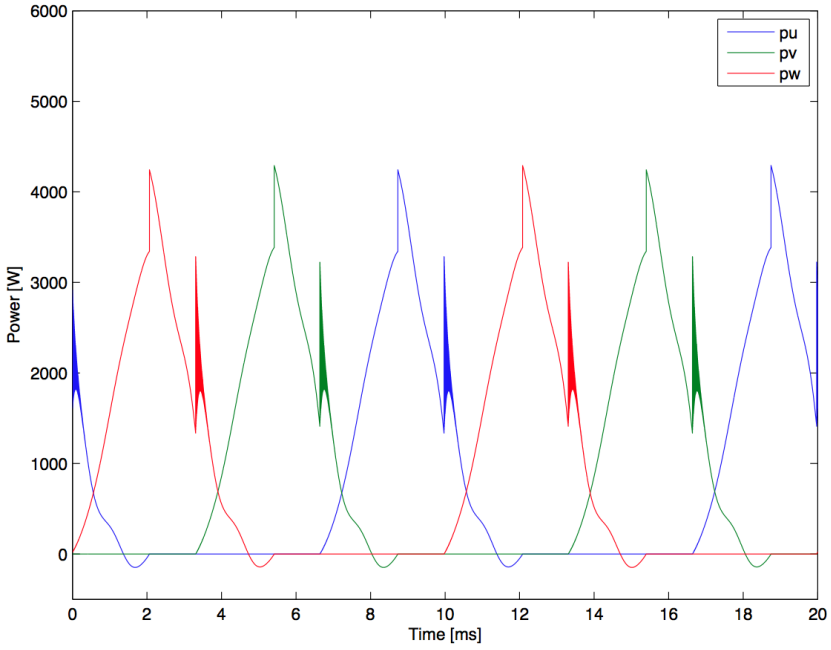

Fig. 5.11 Instantaneous power for each phase, no dotted phases

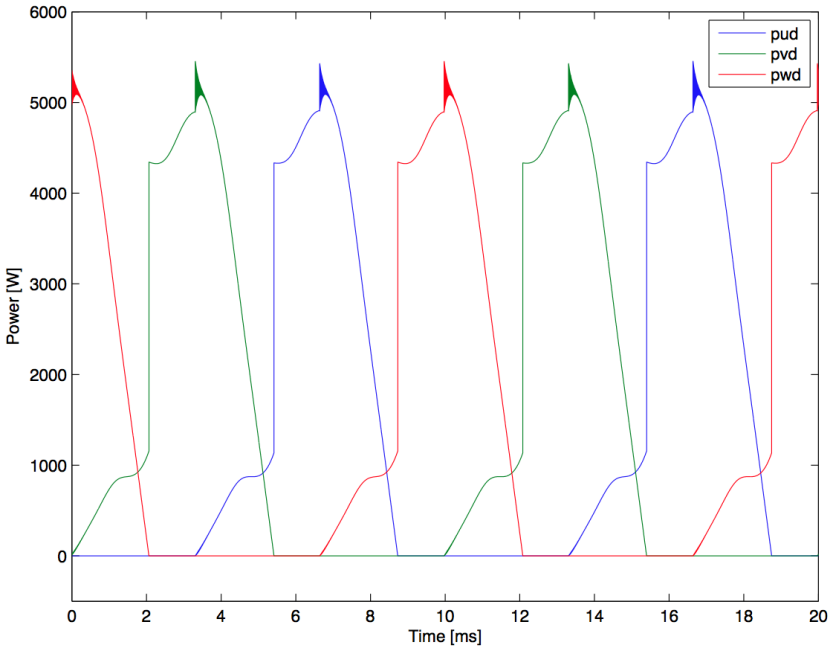

Fig. 5.12 Instantaneous power for each phase, dotted phases

The torque variation (figure 5.13) is still big for the six phase system. The relation between the load power and the varying input power is shown in figure 5.14.

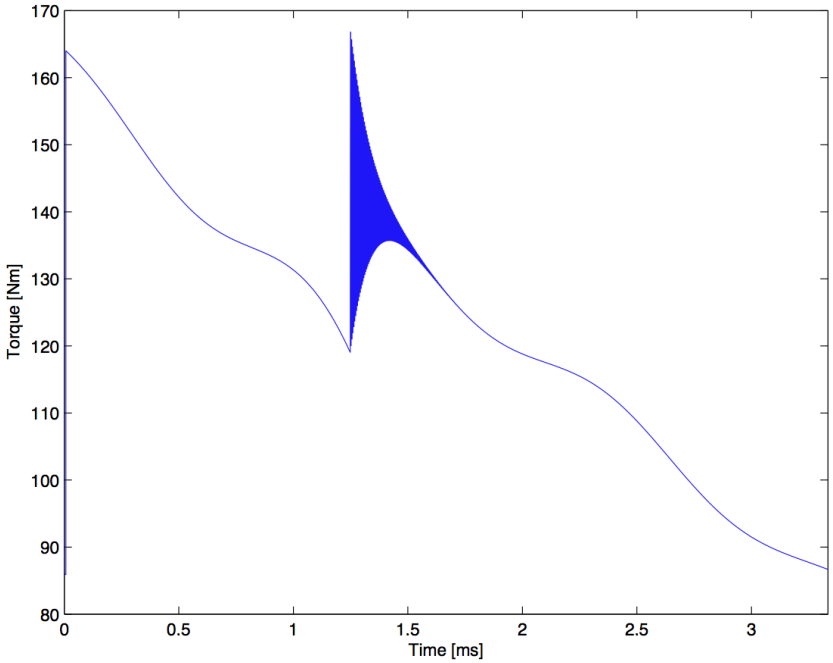

Fig. 5.13 Instantaneous torque variation, full load

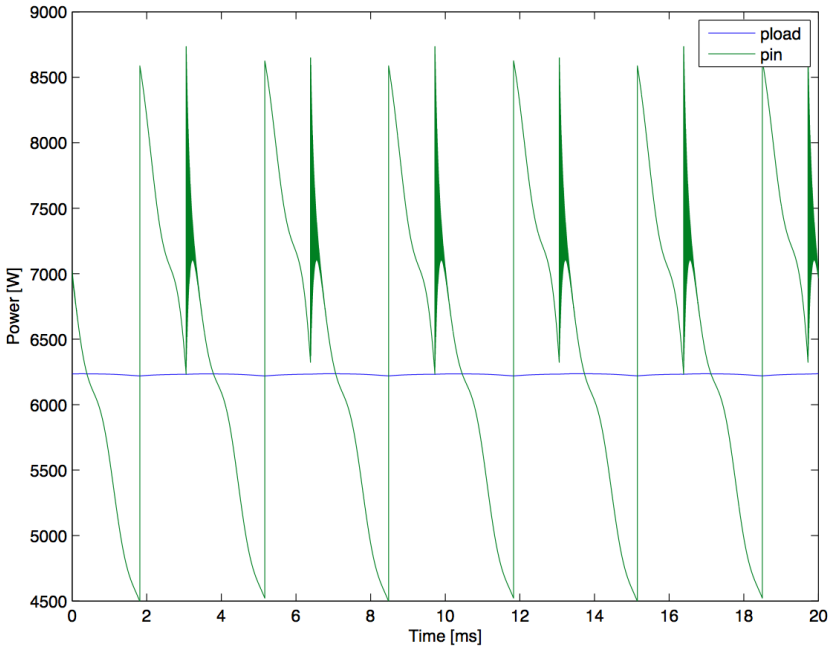

Fig. 5.14 Instantaneous power generation and load consumption

5.4 Comparison between six phase and three phase simulations

This section is about comparing the three phase system and the six phase system to difference in voltage, current, commutation time and torque. The comparison between the three phase and the six phase system shows that the commutation process is faster for the six phase system (see figure 5.18). This results in less magnetic energy accumulation, which causes a lower torque ripple for low angles (see figure 5.19). For unrealistically high steady state delay angles, the torque ripple becomes higher for the six phase system (above 45 degrees).

The ripple in the load current is not so much to worry about since it is constantly low for all simulated delay angles (see figure 5.20). Figure 5.16 shows that the no load voltage is very different from the full load voltage for the same delay angle. This is because a lot of the voltage is lost in the armature reaction.

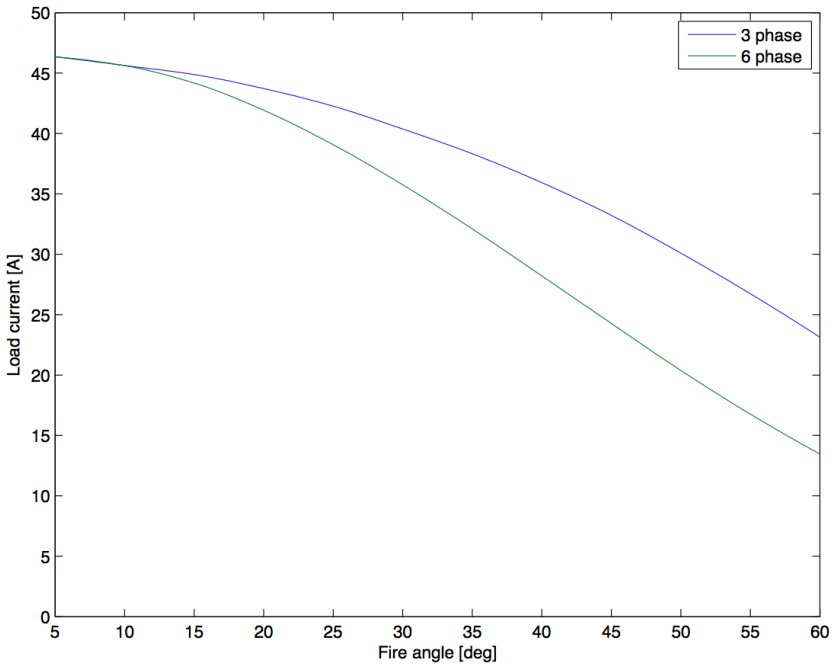

Fig. 5.15 Comparison, load current

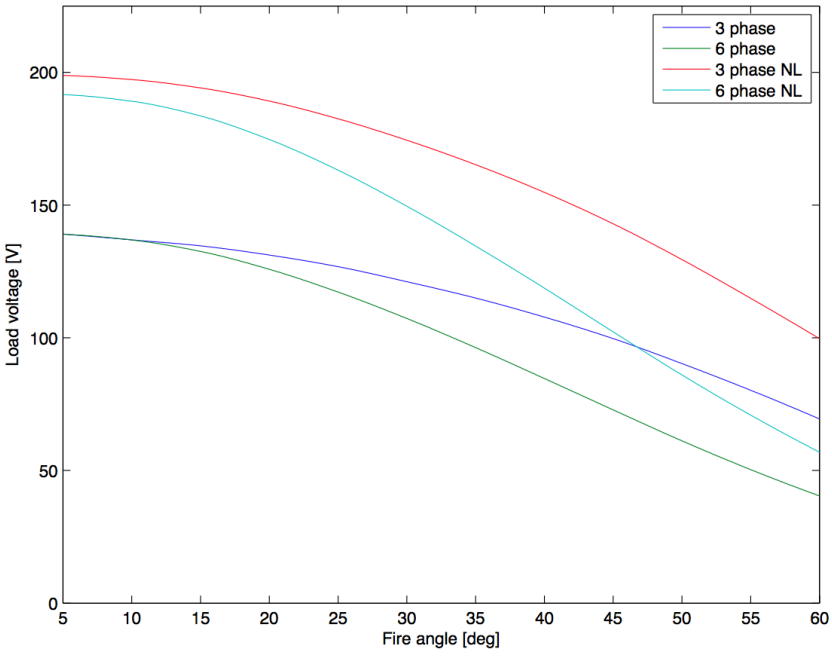

Fig. 5.16 Comparison, load voltage

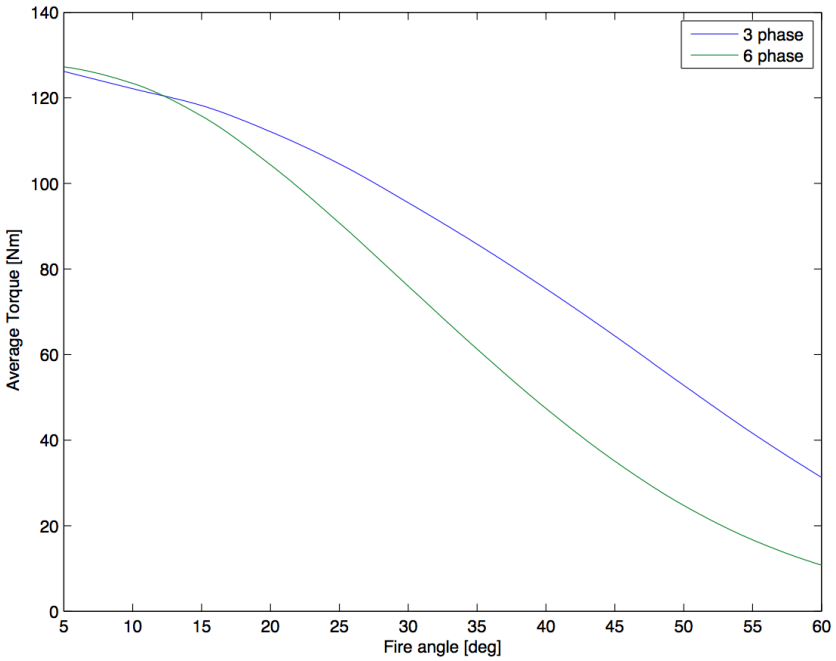

Fig. 5.17 Comparison, Average torque

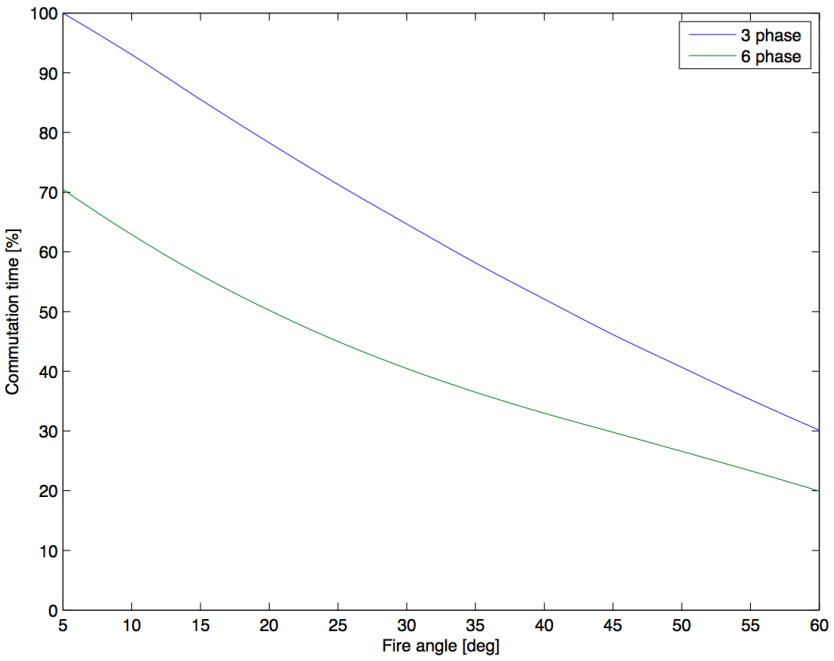

Fig. 5.18 Comparison, commutation time

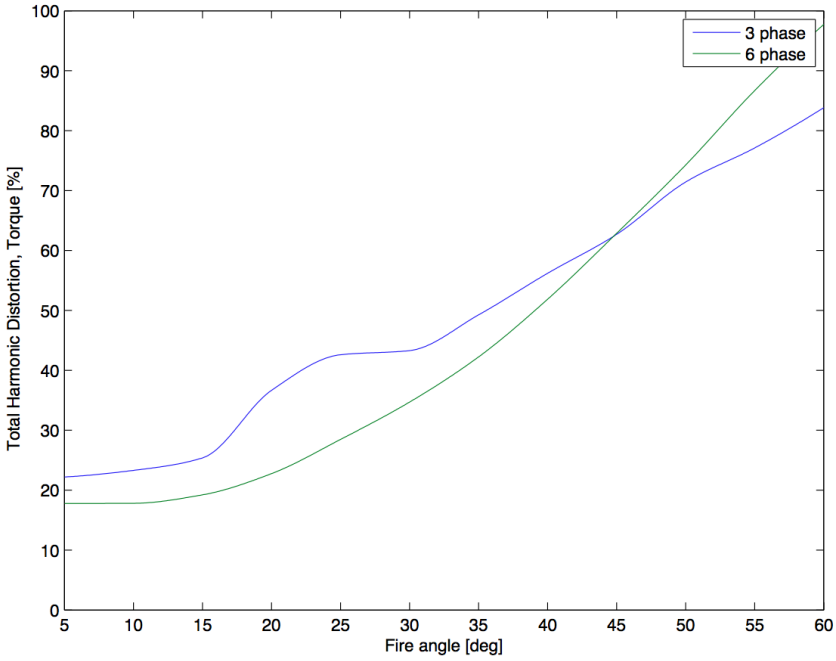

Fig. 5.19 Comparison, torque ripple

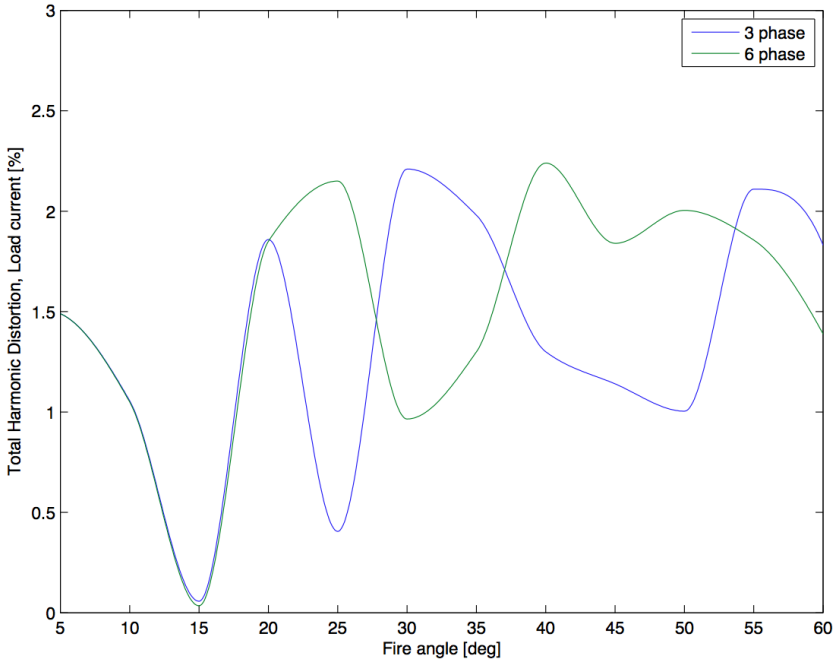

Fig. 5.20 Comparison, current ripple

Chapter 6

Conclusions

The thesis was shown to be more complicated than what was assumed in the beginning of the project. The first goal was to build a coupled FEM and circuit equation model to account for all non-linear effects. It was hard to get convergence with the coupled simulation method.

Therefore ACE was used to find the time-dependent self and mutual inductances between the phases. Because the core material was simulated to be far from saturation for all operating conditions, the inductance linearization was shown to be a very good approximation. The no load voltage waveforms also came from the FEM simulation in ACE. The same geometry was investigated in COMSOL as well with similar results.

The analytical calculations in chapter 2 (results shown in chapter 5) was shown to be close to the results from FEM in chapter 3. The results were close in both magnetic flux density and no-load voltage. The only hard thing to figure out was the flux leakage in the magnetic circuit. The leakage is introduced because the permanent magnets are not placed over the whole pole of the exciter, which creates more circulating fluxes and makes the simple magnetic circuit approximation less valid. The leakage became even worse for the magnetic flux density created by the current in the rotor windings. In that magnetic circuit, the leakage flux was not the minor part of the circuit, but the major part of the circuit. This made the inductance calculation hard. The air gap was very big (compared to normal electrical machines) and most of the flux from the currents in the windings circulated without moving in to the stator core. This in combination with the rotor winding design made the self and mutual inductances to be very high (this is confirmed by measurements and analytical calculations in chapter 2).

The high inductances made the commutation process very slow, which again resulted in a lot of magnetic energy accumulation (reactive power). The load power at the dc side was shown to be very stiff, but the exciter torque is produced as a result of the power consumed on the ac side of the exciter, not the dc side. Because of the high amount of reactive power, the torque ripple on the exciter shaft was shown to be huge, even for low delay angles. Comparisons made between the three phase and the six phase system shows that it is actually possible to reduce the torque ripple. It is possible that with a better design of the exciter, the comparison of the three phase and the six phase system will turn out differently.

An alternative design solution is proposed in the appendix A.5. There it is shown that it is possible to reduce the self inductance with up to 75 percent. A air gap minimum distance of about 4mm is the limiting factor for further reductions.

6.1 Future Work

In the future a new design of the exciter should be done to reduce the magnetic energy oscillations. FEM simulations should be done on the proposed alternative designs (or even other designs as well). A new optimal combination of air gap distance and number of conductors per slot in the rotor should be verified in FEM. Also more advanced simulations with a double three phase series connection should be done with different firing angles at the top and the bottom bridge. The stator could be improved by some adjustable electromagnets in addition to the permanent magnets to increase complexity, but to be able to analyze more solutions for the exciter design.

References

[1] P. T. Amrhein, M.; Krein, *3-D Magnetic Euivalent Circuit Framework for Modeling Electromechanical Devices*. IEEE Transactions on Energy Conversion, vol. 24, no. 2, June 2009, 2009.

[2] A. Arkkio, *Analysis of Induction Motors Based on the Numerical Solution of the Magnetic Field and Circuit Equations*. Helsinki University of Technology, Laboratory of Electromechanics, 1987.

[3] T. I. P. Bondeson, A.; Rylander, *Computational Electromagnetics*. Gothenburg, SWE: Springer, 2005.

[4] L. A. O. V. D. Brauer, J. R..; Larkin, *Finite Element Modeling of Permanent Magnet Devices*. AIP - Journal of Applied Physics, 1984.

[5] P. Butros, *Simulations of Rotating Brushless AC Excitation System with Controlled Thyristor Bridge Rectifier for Hydropower Generators*. Uppsala Universitet, VG Power, 2012.

[6] H. Duane, *Brushless Permanent Magnet Motor Design*. Orono, Main, US: Magna Physics Publishing, 2006.

[7] T. Lipo, *Introduction to AC Machine Design*. US: University of Wisconsin, 2007.

[8] ——, *Analysis of Synchronous Machines*. US: CRC Press, 2012.

[9] J. Luomi, *Magnetic field calculations and electrical machines*. Lecture Notes, 1997.

[10] H. H. K. Malalasekera, W.; Versteeg, *An Introduction to Computational Fluid Dynamics - The Finite Volume Method*. Pearson, Prentice Hall, 2007.

[11] T. V. Pyrhonen, J.;Jokinen, *Design of Rotating Electrical Machines*. Helsinki, Finland: John Wiley Sons Ltd, 2006.

[12] T. W. Reece, A. B. J..;Preston, *Finite Element Methods in Electrical Power Engineering*. United Kingdom: Oxford Science Publications, 2006.

[13] T. Toftevaag, *Excitation and Voltage Control Course*. Energi Norge, SINTEF Energy Reasearch, 2012.

Appendix A

A.1 Finite Difference Method

The finite difference method is based on Taylor expansion [3]:

$$f(x+h) = f(x) + hf'(x) + \frac{h^2}{2}f''(x) + \frac{h^3}{6}f'''(x) + \frac{h^4}{24}f''''(x) \tag{A.1}$$

$$f(x-h) = f(x) - hf'(x) + \frac{h^2}{2}f''(x) - \frac{h^3}{6}f'''(x) + \frac{h^4}{24}f''''(x) \tag{A.2}$$

In this application, second derivative is treated in the differential equations. The second derivative can be approximated like this:

$$\frac{f(x+h) - 2f(x) + f(x-h)}{h^2} = f''(x) + O(h^2) \tag{A.3}$$

Insertion of the taylor expansions into the equation gives the following error function:

$$O(h^2) = \frac{h^2}{12}f''''(x) \tag{A.4}$$

The discretization technique is second order accurate. It means that if the step size (h) is half, the error is one fourth. The finite difference method in 2D solves (in this application) an equation like this:

$$\frac{\partial^2 f(x,y)}{\partial x^2} + \frac{\partial^2 f(x,y)}{\partial y^2} = C \tag{A.5}$$

The obtained discretized equation is then:

$$\frac{f(x+h,y) + f(x-h,y) + f(x,y+h) + f(x,y-h) - 4f(x,y)}{h^2} = C \tag{A.6}$$

In discretized matrix notation:

$$\frac{f_{i+1,j} + f_{i-1,j} + f_{i,j+1} + f_{i,j-1} - 4f_{i,j}}{h^2} = C \tag{A.7}$$

Magnetic scalar potential in 2D (with uniform mesh, constant permeability and without source term):

$$\Omega_{i+1,j} + \Omega_{i-1,j} + \Omega_{i,j+1} + \Omega_{i,j-1} - 4\Omega_{i,j} = 0 \tag{A.8}$$

Magnetic vector potential in 2D:

$$A_{i+1,j} + A_{i-1,j} + A_{i,j+1} + A_{i,j-1} - 4A_{i,j} = -\mu_0\mu_r h^2 J_z \tag{A.9}$$

One way of solving the equations, is by using the Gauss-Seidel numerical method:

$$\Omega_{i,j}^{n+1} = \frac{1}{4}(\Omega_{i+1,j}^{n} + \Omega_{i-1,j}^{n} + \Omega_{i,j+1}^{n} + \Omega_{i,j-1}^{n}) \tag{A.10}$$

$$A_{i,j}^{n+1} = \frac{1}{4}(A_{i+1,j}^{n} + A_{i-1,j}^{n} + A_{i,j+1}^{n} + A_{i,j-1}^{n} + \mu_0\mu_r h^2 J_z) \tag{A.11}$$

The new value of a given cell is computed by the old values of the neighboring cells. To be able to solve for a domain; boundary conditions should be applied on all edges (east, west, south, north). With the Dirichlet condition, the values are specified at the boundary. With the Neuman condition, the derivative is specified at the boundary.

A.2 Finite Volume Method

A more modern version of the finite difference method is the finite volume method. The method is used a lot in computational fluid dynamics [10].

$$\int_s^n \int_w^e \frac{\partial}{\partial x}\left[\nu \frac{\partial A}{\partial x}\right] dxdy + \int_s^n \int_w^e \frac{\partial}{\partial y}\left[\nu \frac{\partial A}{\partial y}\right] dxdy = \int_s^n \int_w^e \frac{\partial H c_x}{\partial y} dxdy - \int_s^n \int_w^e \frac{\partial H c_y}{\partial x} dxdy \tag{A.12}$$

$$(\left[\nu \frac{\partial A}{\partial x}\right]_e - \left[\nu \frac{\partial A}{\partial x}\right]_w)\Delta y + (\left[\nu \frac{\partial A}{\partial y}\right]_n - \left[\nu \frac{\partial A}{\partial y}\right]_s)\Delta x = (Hc_{x,n} - Hc_{x,s})\Delta x + (Hc_{y,e} - Hc_{y,w})\Delta y \tag{A.13}$$

$$\left[\frac{\nu_e \Delta y}{\partial x_e}\right](A_E - A_P) - \left[\frac{\nu_w \Delta y}{\partial x_w}\right](A_P - A_W) + \left[\frac{\nu_n \Delta x}{\partial y_n}\right](A_N - A_P) - \left[\frac{\nu_s \Delta x}{\partial y_s}\right](A_P - A_S) = (Hc_{x,n} - Hc_{x,s})\Delta x + (Hc_{y,e} - Hc_{y,w})\Delta \tag{A.14}$$

Each point can be solved by Gauss Seidel iteration, by treating the neighbor potentials as constant and solve for the point [10]

$$A_P = \frac{c_W A_W + c_E A_E + c_S A_S + c_N A_N + S_U}{c_P} \tag{A.15}$$

where:

$$c_W = \frac{\nu_w \Delta y}{\partial x_w} \tag{A.16}$$

$$c_E = \frac{\nu_e \Delta y}{\partial x_e} \tag{A.17}$$

$$c_S = \frac{\nu_s \Delta x}{\partial y_s} \tag{A.18}$$

$$c_N = \frac{\nu_n \Delta x}{\partial y_n} \tag{A.19}$$

$$c_P = c_W + c_E + c_S + c_N \tag{A.20}$$

$$S_U = (Hc_{x,n} - Hc_{x,s})\Delta x + (Hc_{y,e} - Hc_{y,w})\Delta y \tag{A.21}$$

An alternative is to make a matrix system of all the equations and solve it by Newton-Raphson method. The number of equations is equal to the number of discretized finite volumes.

A.3 Finite Element Method

Instead of defining discretized points, the finite element method defines entire elements. The shape and size of the elements can vary throughout the whole domain. The elements are often made as triangles with either linear, quadratic or cubic shape functions to describe the potential along the element [7].
Linear shape function:

$$f(x, y) = \alpha_1 + \alpha_2 x + \alpha_3 y \tag{A.22}$$

Quadratic shape function:

$$f(x, y) = \alpha_1 + \alpha_2 x + \alpha_3 y + \alpha_4 x^2 + \alpha_5 y^2 \tag{A.23}$$

Cubic shape function:

$$f(x, y) = \alpha_1 + \alpha_2 x + \alpha_3 y + \alpha_4 x^2 + \alpha_5 y^2 + \alpha_6 x^3 + \alpha_7 y^3 \tag{A.24}$$

The linear function has three unknown coefficients, the quadratic has five and the cubic has seven. Each element needs the solver to compute for the same number of points in the elements as the number of unknown coefficients. To solve for the coefficients of the linear shape function, one uses the computed values from the three corners of the element triangle. This gives three equations, three knowns and three unknowns:

$$f_i = \alpha_1 + \alpha_2 x_i + \alpha_3 y_i \tag{A.25}$$

$$f_j = \alpha_1 + \alpha_2 x_j + \alpha_3 y_j \tag{A.26}$$

$$f_k = \alpha_1 + \alpha_2 x_k + \alpha_3 y_k \tag{A.27}$$

A.3.1 Variational Method

The variational method is an energy method that utilizes the information about the energy in the magnetic field [7]. For linear materials, magnetic energy is:

$$w_{mag} = \frac{1}{2}\mathbf{B}\cdot\mathbf{H} = \frac{1}{2}\mu_0\mu_r|\mathbf{H}|^2 = \frac{1}{2}\frac{|\mathbf{B}|^2}{\mu_0\mu_r} \tag{A.28}$$

In the general case if the material is non-linear:

$$w_{mag} = \int_0^{\mathbf{B}} \mathbf{H}\cdot d\mathbf{B} \tag{A.29}$$

The magnetic energy density is expressed in joules per meter cube. A more complete expression for the system energy can be found from the following vector identity:

$$\nabla\cdot(\mathbf{E}\times\mathbf{H}) = \mathbf{H}\cdot(\nabla\times\mathbf{E}) - \mathbf{E}\cdot(\nabla\times\mathbf{H}) \tag{A.30}$$

The identity can be simplified with Faraday's law and Ampere's law, neglecting displacement currents.

$$\nabla\cdot(\mathbf{E}\times\mathbf{H}) = -\mathbf{H}\cdot\frac{d\mathbf{B}}{dt} - \mathbf{J}\cdot\mathbf{E} \tag{A.31}$$

$$\nabla\cdot(\mathbf{E}\times\mathbf{H}) + \mathbf{H}\cdot\frac{d\mathbf{B}}{dt} + \mathbf{J}\cdot\mathbf{E} = 0 \tag{A.32}$$

$$\int_V \nabla\cdot(\mathbf{E}\times\mathbf{H})dV + \int_V \mathbf{H}\cdot\frac{d\mathbf{B}}{dt}dV + \int_V \mathbf{J}\cdot\mathbf{E}dV = 0 \tag{A.33}$$

Gauss's theorem:

$$\oint_S \mathbf{E}\times\mathbf{H}\cdot d\mathbf{S} + \int_V \mathbf{H}\cdot\frac{d\mathbf{B}}{dt}dV + \int_V \mathbf{J}\cdot\mathbf{E}dV = 0 \tag{A.34}$$

The cross product of the E-field and the H-field has only a z-component, and the net flux of it out of the volume is zero.

$$\int_V \mathbf{H}\cdot\frac{d\mathbf{B}}{dt}dV + \int_V \mathbf{J}\cdot\mathbf{E}dV = 0 \tag{A.35}$$

Insertion of the definition of the magnetic vector potential into Faraday's law gives:

$$\nabla\times\mathbf{E} = -\frac{\partial}{\partial t}(\nabla\times\mathbf{A}) \tag{A.36}$$

By assuming negligible electrostatic potential:

$$\mathbf{E} = -\frac{\partial\mathbf{A}}{\partial t} \tag{A.37}$$

This equation can be used for simplification.

$$\int_V \mathbf{H}\cdot\frac{d\mathbf{B}}{dt}dV - \int_V \mathbf{J}\cdot\frac{\partial\mathbf{A}}{\partial t}dV = 0 \tag{A.38}$$

$$\frac{\partial}{\partial t}\int_V \left[\int_0^{\mathbf{B}} \mathbf{H}\cdot d\mathbf{B}\right] dV - \frac{\partial}{\partial t}\int_V \left[\int_0^{\mathbf{A}} \mathbf{J}\cdot d\mathbf{A}\right] dV = 0 \tag{A.39}$$

$$\frac{\partial}{\partial t}W_{mag} + \frac{\partial}{\partial t}W_e = P_{mag} + P_e = 0 \tag{A.40}$$

A converged solution is found when the sum of the electrical and magnetic energy is maximized, because then the power balance equation is statisfied.

$$w_{mag} = \int_0^{\mathbf{B}} \mathbf{H}\cdot d\mathbf{B} = \int_0^{B_x} H_x dB_x + \int_0^{B_y} H_y dB_y \tag{A.41}$$

$$w_e = -\mathbf{J} \cdot \mathbf{A} = -J_z A_z \tag{A.42}$$

For linear materials, the magnetic energy integral simplifies to

$$w_{mag} = \frac{B_x^2 + B_y^2}{2\mu_0 \mu_r} \tag{A.43}$$

The magnetic energy function can be expressed for both scalar potential and vector potential in 2D.

$$w_{mag} = \frac{1}{2\mu_0 \mu_r} \left[\left(\frac{\partial A_z}{\partial x} \right)^2 + \left(\frac{\partial A_z}{\partial y} \right)^2 \right] \tag{A.44}$$

$$w_{mag} = \frac{\mu_0 \mu_r}{2} \left[\left(\frac{\partial \Omega}{\partial x} \right)^2 + \left(\frac{\partial \Omega}{\partial y} \right)^2 \right] \tag{A.45}$$

$$F = \int_S (w_{mag} + w_e) dS \tag{A.46}$$

The function F (joule per meter) should have a zero derivative with respect to every node potential in every triangle in the whole domain you solve for.

A linear shape function describes the magnetic vector potential along the element.

$$A = \alpha_1 + \alpha_2 x + \alpha_3 y \tag{A.47}$$

The vector potential at the three nodes of the triangular element must be:

$$A_i = \alpha_1 + \alpha_2 x_i + \alpha_3 y_i \tag{A.48}$$

$$A_j = \alpha_1 + \alpha_2 x_j + \alpha_3 y_j \tag{A.49}$$

$$A_k = \alpha_1 + \alpha_2 x_k + \alpha_3 y_k \tag{A.50}$$

This system of equations can be written in matrix form:

$$\begin{bmatrix} A_i \\ A_j \\ A_k \end{bmatrix} = \begin{bmatrix} 1 & x_i & y_i \\ 1 & x_j & y_j \\ 1 & x_k & y_k \end{bmatrix} \begin{bmatrix} \alpha_1 \\ \alpha_2 \\ \alpha_3 \end{bmatrix} \tag{A.51}$$

By matrix inversion, one can obtain the coefficients.

$$\begin{bmatrix} \alpha_1 \\ \alpha_2 \\ \alpha_3 \end{bmatrix} = \begin{bmatrix} 1 & x_i & y_i \\ 1 & x_j & y_j \\ 1 & x_k & y_k \end{bmatrix}^{-1} \begin{bmatrix} A_i \\ A_j \\ A_k \end{bmatrix} \tag{A.52}$$

The inversion can be made efficiently by Cramers rule and then the matrix looks like this:

$$\begin{bmatrix} \alpha_1 \\ \alpha_2 \\ \alpha_3 \end{bmatrix} = \frac{1}{2\Delta} \begin{bmatrix} a_i & a_j & a_k \\ b_i & b_j & b_k \\ c_i & c_j & c_k \end{bmatrix} \begin{bmatrix} A_i \\ A_j \\ A_k \end{bmatrix} \tag{A.53}$$

The solved coefficients are:

$$a_i = x_j y_k - x_k y_j \tag{A.54}$$

$$a_j = x_k y_i - x_i y_k \tag{A.55}$$

$$a_k = x_i y_j - x_j y_i \tag{A.56}$$

$$b_i = y_j - y_k \tag{A.57}$$

$$b_j = y_k - y_i \tag{A.58}$$

$$b_k = y_i - y_j \tag{A.59}$$

$$c_i = x_k - x_j \tag{A.60}$$

$$c_j = x_i - x_k \tag{A.61}$$

$$c_k = x_j - x_i \tag{A.62}$$

$$\Delta = \frac{1}{2}\left[(x_j y_k - x_k y_j) + x_i(y_j - y_k) + y_i(x_k - x_j)\right] \tag{A.63}$$

It is interesting to notice that Δ is didactically equal to the area of the triangle element defined by the nodes i, j and k. The coefficients are then:

$$\alpha_1 = \frac{1}{2\Delta}(a_i A_i + a_j A_j + a_k A_k) \tag{A.64}$$

$$\alpha_2 = \frac{1}{2\Delta}(b_i A_i + b_j A_j + b_k A_k) \tag{A.65}$$

$$\alpha_3 = \frac{1}{2\Delta}(c_i A_i + c_j A_j + c_k A_k) \tag{A.66}$$

The derived coefficients can be inserted into the general shape function.

$$A = \frac{1}{2\Delta}\left[(a_i A_i + a_j A_j + a_k A_k) + (b_i A_i + b_j A_j + b_k A_k)x + (c_i A_i + c_j A_j + c_k A_k)y\right] \tag{A.67}$$

$$A = \frac{1}{2\Delta}\left[(a_i + b_i x + c_i y)A_i + (a_j + b_j x + c_j y)A_j + (a_k + b_k x + c_k y)A_k\right] \tag{A.68}$$

$$A = N_i A_i + N_j A_j + N_k A_k \tag{A.69}$$

$$A = \begin{bmatrix} N_i & N_j & N_k \end{bmatrix} \begin{bmatrix} A_i \\ A_j \\ A_k \end{bmatrix} \tag{A.70}$$

$$N_i = \frac{1}{2\Delta}(a_i + b_i x + c_i y) \tag{A.71}$$

$$N_j = \frac{1}{2\Delta}(a_j + b_j x + c_j y) \tag{A.72}$$

$$N_k = \frac{1}{2\Delta}(a_k + b_k x + c_k y) \tag{A.73}$$

The N-functions make an interpolation of the point with respect to the defined node potentials. At the point (x_i, y_i), $N_i = 1$, $N_j = 0$ and $N_k = 0$. At the point (x_j, y_j), $N_i = 0$, $N_j = 1$ and $N_k = 0$. At the point (x_k, y_k), $N_i = 0$, $N_j = 0$ and $N_k = 1$. From the definition of the vector potential, the numerical solution of the magnetic flux density can be solved.

$$B_x = \frac{\partial A}{\partial y} \tag{A.74}$$

$$B_y = -\frac{\partial A}{\partial x} \tag{A.75}$$

$$B_x = \frac{1}{2\Delta}(c_i A_i + c_j A_j + c_k A_k) \tag{A.76}$$

$$B_y = -\frac{1}{2\Delta}(b_i A_i + b_j A_j + b_k A_k) \tag{A.77}$$

The magnitude of the magnetic field:

$$|B| = \sqrt{B_x^2 + B_y^2} \tag{A.78}$$

$$|B| = \frac{1}{2\Delta}\sqrt{(b_i A_i + b_j A_j + b_k A_k)^2 + (c_i A_i + c_j A_j + c_k A_k)^2} \tag{A.79}$$

Note that the magnetic flux density B is constant over the triangle. Since the reluctivity is a function of the amplitude of B, it is evident that ν is also constant over the region.

$$\nu = \frac{1}{\mu_0 \mu_r} = \frac{|H|}{|B|} \tag{A.80}$$

$$|H| = f(|B|) \tag{A.81}$$

The magnetizing force H is fund by interpolation from the BH-curve for the material you solve for. The function that should be minimized is:

$$F = \int_S \left(\frac{\nu}{2} \left[\left(\frac{\partial A}{\partial x} \right)^2 + \left(\frac{\partial A}{\partial y} \right)^2 \right] - JA \right) dS \tag{A.82}$$

$$\frac{\partial F}{\partial A_i} = \frac{\partial F}{\partial A_j} = \frac{\partial F}{\partial A_k} = 0 \tag{A.83}$$

$$\frac{\partial F}{\partial A_i} = \int_S \left(\nu \left[\frac{\partial A}{\partial x} \frac{\partial}{\partial A_i} \left(\frac{\partial A}{\partial x} \right) + \frac{\partial A}{\partial y} \frac{\partial}{\partial A_i} \left(\frac{\partial A}{\partial y} \right) \right] - J \frac{\partial A}{\partial A_i} \right) dS \tag{A.84}$$

The components of the discretizated vector potential gradient is:

$$\frac{\partial A}{\partial x} = \frac{1}{2\Delta}(b_i A_i + b_j A_j + b_k A_k) \tag{A.85}$$

$$\frac{\partial A}{\partial y} = \frac{1}{2\Delta}(c_i A_i + c_j A_j + c_k A_k) \tag{A.86}$$

After differentiation with respect to the node potential:

$$\frac{\partial}{\partial A_i} \left(\frac{\partial A}{\partial x} \right) = \frac{b_i}{2\Delta} \tag{A.87}$$

$$\frac{\partial}{\partial A_i} \left(\frac{\partial A}{\partial y} \right) = \frac{c_i}{2\Delta} \tag{A.88}$$

$$\frac{\partial A}{\partial A_i} = N_i \tag{A.89}$$

$$\frac{\partial F}{\partial A_i} = \frac{1}{2\Delta} \int_S \left(\frac{\nu}{2\Delta} \left[b_i(b_i A_i + b_j A_j + b_k A_k) + c_i(c_i A_i + c_j A_j + c_k A_k) \right] - J(a_i + b_i x + c_i y) \right) dS \tag{A.90}$$

$$\frac{\partial F}{\partial A_i} = \frac{\nu}{4\Delta} \left[b_i(b_i A_i + b_j A_j + b_k A_k) + c_i(c_i A_i + c_j A_j + c_k A_k) \right] - \frac{J}{2\Delta} \int_S (a_i + b_i x + c_i y) dS \tag{A.91}$$

Since the integration over the area of a triangle is equivalent to integrating a weighted function at its centroid, one can write:

$$\int_S (a_i + b_i x + c_i y) dS = \int_S (a_i + b_i \overline{x} + c_i \overline{y}) dS \tag{A.92}$$

The weighted coordinated can be viewed as the ”centre of gravity” of the triangle.

$$\overline{x} = \frac{x_i + x_j + x_k}{3} \tag{A.93}$$

$$\overline{y} = \frac{y_i + y_j + y_k}{3} \tag{A.94}$$

Finally it can be proven that:

$$\int_S (a_i + b_i x + c_i y) dS = \frac{2\Delta^2}{3} \tag{A.95}$$

This simplifies the final equation:

$$\frac{\partial F}{\partial A_i} = \frac{\nu}{4\Delta} \left[b_i(b_i A_i + b_j A_j + b_k A_k) + c_i(c_i A_i + c_j A_j + c_k A_k) \right] - \frac{J\Delta}{3} \tag{A.96}$$

The minimized function for the other nodes in the triangle becomes very similar. All of them can be put into a matrix together.

$$\begin{bmatrix} \frac{\partial F}{\partial A_i} \\ \frac{\partial F}{\partial A_j} \\ \frac{\partial F}{\partial A_k} \end{bmatrix} = \frac{\nu}{4\Delta} \begin{bmatrix} b_i^2 + c_i^2 & b_i b_j + c_i c_j & b_i b_k + c_i c_k \\ b_i b_j + c_i c_j & b_j^2 + c_j^2 & b_j b_k + c_j c_k \\ b_i b_k + c_i c_k & b_j b_k + c_j c_k & b_k^2 + c_k^2 \end{bmatrix} \begin{bmatrix} A_i \\ A_j \\ A_k \end{bmatrix} - \frac{J\Delta}{3} \begin{bmatrix} 1 \\ 1 \\ 1 \end{bmatrix} = \begin{bmatrix} 0 \\ 0 \\ 0 \end{bmatrix} \tag{A.97}$$

The product of the current density (J) and the area of the triangle (Δ) gives the total current flowing through the triangle.

$$\frac{\nu}{4\Delta}\begin{bmatrix} b_i^2+c_i^2 & b_ib_j+c_ic_j & b_ib_k+c_ic_k \\ b_ib_j+c_ic_j & b_j^2+c_j^2 & b_jb_k+c_jc_k \\ b_ib_k+c_ic_k & b_jb_k+c_jc_k & b_k^2+c_k^2 \end{bmatrix}\begin{bmatrix} A_i \\ A_j \\ A_k \end{bmatrix} = \frac{1}{3}\begin{bmatrix} I \\ I \\ I \end{bmatrix} \tag{A.98}$$

The matrix equation can be written more compactly:

$$\begin{bmatrix} S_{ii} & S_{ij} & S_{ik} \\ S_{ji} & S_{jj} & S_{jk} \\ S_{ki} & S_{kj} & S_{kk} \end{bmatrix}\begin{bmatrix} A_i \\ A_j \\ A_k \end{bmatrix} = \frac{1}{3}\begin{bmatrix} I \\ I \\ I \end{bmatrix} \tag{A.99}$$

This matrix gives a relationship between the nodes in an element. Some of the same nodes are part of neighboring elements. By numerating the nodes and adding all the matrixes together, one will obtain the so called stiffness matrix. Since FEM is an evolved technique originating from structural mechanics the name of the matrix doesn't make so much sense. Therefore in magnetic fields it is also called the reluctivity matrix.

A.4 Comparision between FVM, MEC and FEM

The exciter was evaluated with the three different methods: FVM, MEC and FEM. The results are similar for a simulation of a half pole of the exciter:

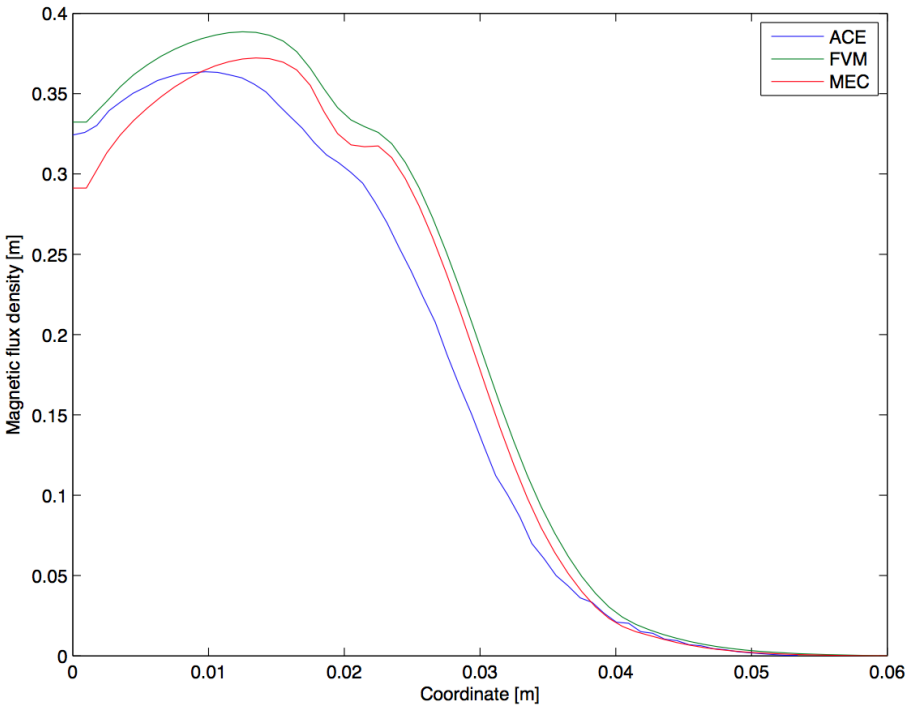

Fig. A.1 Comparision of the solved static magnetic field for a half pole with FVM, MEC and FEM

All the flux is simulated to flow between the neighboring poles and with a symmetry line a the middle of a pole. No magnetic flux cross that line for a static simulation. For FVM and FEM, zero vector potential is implemented and for MEC Neumann condition is implemented. In the border between the poles Neumann is implemented for FVM and FEM, but zero reference scalar potential is implemented for MEC.

A.5 Alternative Designs

In the alternative design evaluation it is used three permanent magnets instead of two. The geometry for the magnetic circuit of the permanent magnets are shown in figure A.2, with the magnetic circuit in figure A.3. The

magnetic circuit for the inductance calculation will be the same as the one derived in chapter 2 of the thesis (with b_3 equal to 3mm). It is important to note that the air gap distance for the permanent magnets are always 3mm smaller than distance between the stator and rotor core. The equivalent air gap for the magnetic circuit of the rotor slot conductor currents, considering that the permanent magnets have a relative permeability close to air, will be around $2.6mm$ larger (averaged value).

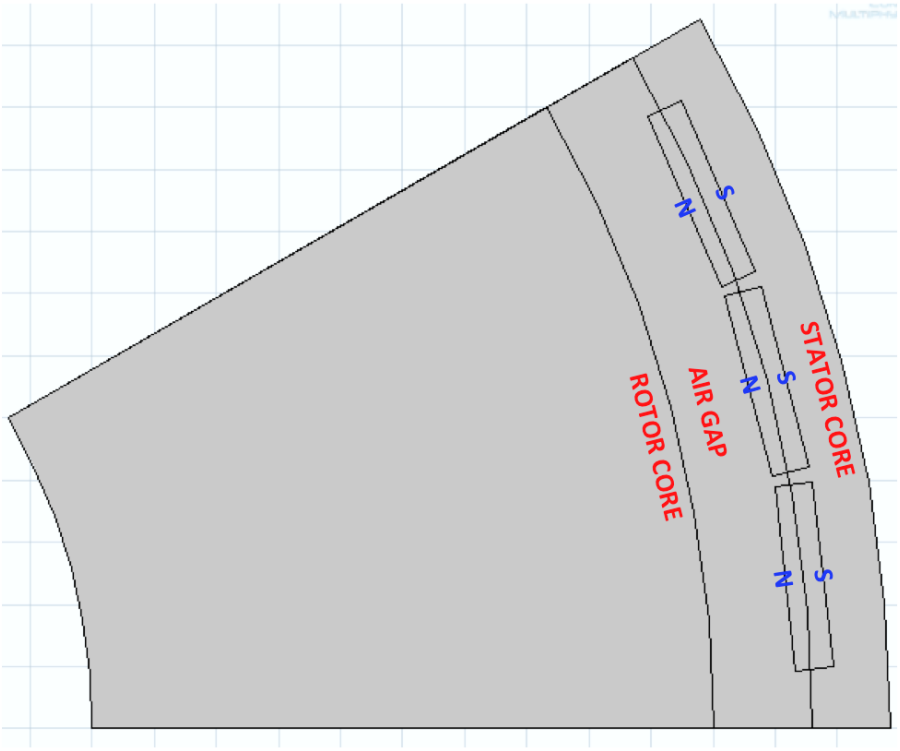

Fig. A.2 Permanent Magnet Geometry

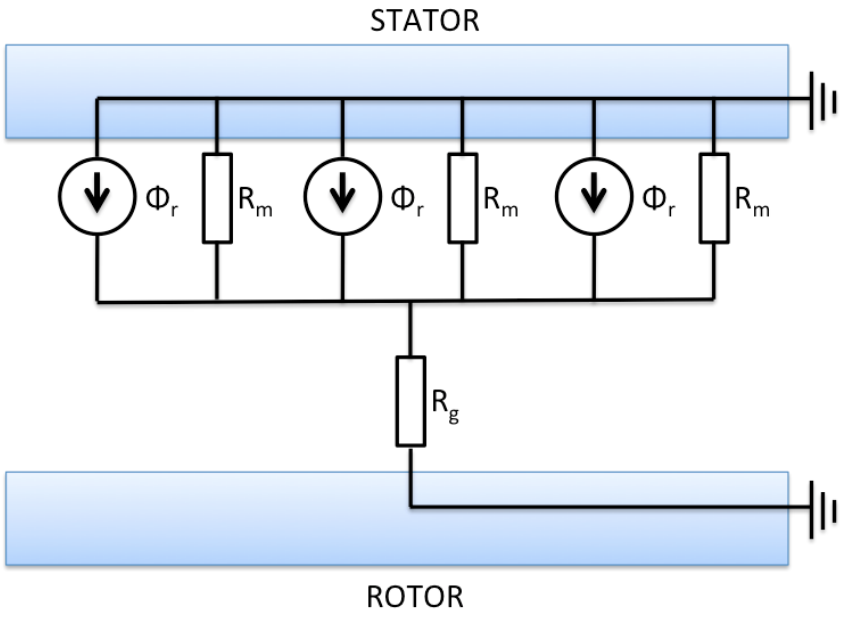

Fig. A.3 Magnetic circuit for the permanent magnets

Using radial flux assumption, the air gap reluctance yields

$$\Re_g = \frac{ln(1+g/r_3)}{\mu_0 l_z \theta_p} \tag{A.100}$$

where

$$\Phi_{r,tot} = 3\Phi_r \tag{A.101}$$

and

$$\Re_{m,tot} = \frac{\Re_m}{3} \tag{A.102}$$

The solution of the air gap flux will then be

$$\Phi_g = \frac{\Re_{m,tot}}{\Re_{m,tot} + \Re_g} \Phi_{r,tot} \tag{A.103}$$

where

$$B_g = \frac{\Phi_g}{l_z \theta_p R} \tag{A.104}$$

The total no load voltage can be found by the flux cutting form of Faradays law, multiplying the voltage induced in each conductor with the number of conductors per slot (N) and a factor depending on the number of parallel circuits (p). This gives

$$U = Nu\frac{2n_p}{p} \tag{A.105}$$

where

$$U = 4\pi B_g N r_3 l_z f \frac{1}{p} \tag{A.106}$$

when the equation 2.20 is inserted. The required air gap flux density for a given voltage (U), a given number of parallel circuits (p) and given number of slot conductors (N), is

$$B_g = \frac{Up}{4\pi N R l_z f} \tag{A.107}$$

The magnetic circuit is tried out for different combinations of the parameters which govern 120V induced no load voltage. The results are shown in A.1.

Table A.1 Magnetic circuit solution and inductance solutions for 120V induced no-load voltage

N	p	g [mm]	B_g [T]	L [mH]
24	2	12	0.40	2.28
22	2	10.5	0.43	1.96
20	2	9	0.48	1.66
18	2	7.3	0.53	1.39
16	2	5.8	0.60	1.15
14	2	4.2	0.68	0.93
12	1	12	0.40	1.14
10	1	9	0.48	0.83
8	1	5.8	0.60	0.57
6	1	2.6	0.80	0.37

Data: $\Re_m = 757881A-turns/Wb, r_3 = 0.2m, l_z = 0.2m, f = 50Hz, n_p = 6, \theta_p = \frac{\pi}{6}, U = 120V$. With no parallel circuits, it is actually possible to reduce the self inductance with a factor of 73 percent. Another issue with this configuration is that the amount of current flowing in the windings will be doubled. With two parallel circuits, approximately 25A will flow in each circuit. With one circuit, 50A has to flow in all conductors. The cross sectional area of the conductor is $7.07mm^2$ with a diameter of 3mm. This yields a current density in the conductors of approximately $7.07A/mm^2$, which is an upper limit of what copper can handle at the specified cooling conditions (natural cooling).